UNIVERSIDADE FEDERAL DE MINAS GERAIS

ENGINEERING SCHOOL

GRADUATE PROGRAM IN MECHANICAL ENGINEERING

JORGE LUIS ORTIZ SOLANO

DEVELOPMENT OF A COMPUTER VISION RECOGNITION TOOL FOR UNDERWATER WET WELDING

Belo Horizonte

2021

Jorge Luis Ortiz Solano

DEVELOPMENT OF A COMPUTER VISION RECOGNITION TOOL FOR UNDERWATER WET WELDING

Final Version

Dissertation presented to the Graduate Program in Mechanical Engineering at the Federal University of Minas Gerais, as a partial requirement for obtaining the Master's degree in Mechanical Engineering.

Area of concentration: Manufacturing Processes

Advisor: Prof. Dr. Ariel Rodríguez Arias

Co-advisor: Prof. Dr. Eduardo José Lima II

Belo Horizonte

2021

Solano, Jorge Luis Ortiz.
S684d Development of a computer vision image recognition tool for underwater wet welding [recurso eletrônico] / Jorge Luis Ortiz Solano. - 2021.
1 recurso online (60 f. : il., color.) : pdf.

Orientador: Ariel Rodriguez Arias.
Coorientador: Eduardo José Lima II.

Dissertação (mestrado) - Universidade Federal de Minas Gerais, Escola de Engenharia.

Apêndices: f. 52-60.

Bibliografia: f. 44-51.
Exigências do sistema: Adobe Acrobat Reader.

1. Engenharia mecânica - Teses. 2. Soldagem subaquática - Teses. 3. Arco de soldagem submersa - Teses. I. Rodríguez Arias, Ariel. II. Lima II, Eduardo José. III. Universidade Federal de Minas Gerais. Escola de Engenharia. IV. Título.

CDU: 621(043)

Ficha catalográfica elaborada pela Bibliotecária Roseli Alves de Oliveira CRB/6 2121
Biblioteca Prof. Mário Werneck, Escola de Engenharia da UFMG

UNIVERSIDADE FEDERAL DE MINAS GERAIS
ESCOLA DE ENGENHARIA
PROGRAMA DE PÓS-GRADUAÇÃO EM ENGENHARIA MECÂNICA

FOLHA DE APROVAÇÃO

DESENVOLVIMENTO DE UMA FERRAMENTA DE RECONHECIMENTO DE VISÃO POR COMPUTADOR PARA SOLDAGEM SUBAQUÁTICA MOLHADA

JORGE LUIS ORTIZ SOLANO

Dissertação submetida à Banca Examinadora designada pelo Colegiado do Programa de Pós-Graduação em Engenharia Mecânica da Universidade Federal de Minas Gerais, constituída pelos Professores: Dr. Ariel Rodriguez Arias (Orientador – Departamento de Engenharia Mecânica/UFMG), Dr. Alexandre Queiroz Bracarense (Professor aposentado do Departamento de Engenharia Mecânica/UFMG) e Dr. Régis Henrique Gonçalves e Silva (Universidade Federal de Santa Catarina/UFSC), como parte dos requisitos necessários à obtenção do título de **"Mestre em Engenharia Mecânica"**, na área de concentração de **"Engenharia de Manufatura e Materiais".**

Dissertação aprovada no dia 22 de julho de 2022.

Documento assinado eletronicamente por **Ariel Rodriguez Arias**, **Professor do Magistério Superior**, em 08/08/2022, às 11:30, conforme horário oficial de Brasília, com fundamento no art. 5º do Decreto nº 10.543, de 13 de novembro de 2020.

Documento assinado eletronicamente por **Alexandre Queiroz Bracarense**, **Membro**, em 08/08/2022, às 13:52, conforme horário oficial de Brasília, com fundamento no art. 5º do Decreto nº 10.543, de 13 de novembro de 2020.

Documento assinado eletronicamente por **Regis Henrique Goncalves e Silva**, **Usuário Externo**, em 17/08/2022, às 12:28, conforme horário oficial de Brasília, com fundamento no art. 5º do Decreto nº 10.543, de 13 de novembro de 2020.

A autenticidade deste documento pode ser conferida no site https://sei.ufmg.br/sei/controlador_externo.php?acao=documento_conferir&id_orgao_acesso_externo=0, informando o código verificador **1629627** e o código CRC **1CF984BB**.

RESUMO

O foco deste trabalho é analisar a dinâmica das bolhas resultantes do processo de soldagem, sobre o efeito de diferentes formulações de eletrodos revestidos, em ambas as polaridades e variando a corrente de soldagem. As análises visuais da formação de bolhas têm sido aceitas como uma ferramenta fundamental no estudo do processo de soldagem devido ao seu efeito de correlação com a estabilidade do processo e, portanto, com o cordão de solda final. Além disso, o processo de soldagem a arco de metal blindado ainda é a técnica dominante utilizada na engenharia naval e submarina devido ao seu custo razoável de implementação e desempenho adequado.

O trabalho proposto inclui o estudo de três diferentes eletrodos em bastão projetados especificamente para soldagem subaquática úmida, incluindo, dois eletrodos desenvolvidos no Laboratório de Robótica, Soldagem e Simulação, e um comercial específico para soldagem subaquática. As diferenças sob polaridade direta e inversa são destacadas pela evolução das bolhas e análise de estabilidade do arco.

Este trabalho é desenvolvido através da utilização de um sistema de imagem de qualidade, uma fonte de alimentação, um sistema de aquisição de dados e um algoritmo de detecção e rastreamento. O algoritmo de processamento de imagem identifica as bolhas geradas nos experimentos de soldagem subaquática a arco de metal blindado. Além disso, o algoritmo facilita o cálculo da área projetada da bolha e seu diâmetro equivalente. Em seguida, é capaz de rastrear as bolhas para fins de monitoramento, bem como calcular sua frequência.

Como o sistema de imagem e o sinal são sincronizados, é possível determinar a relação entre as bolhas e as características elétricas do arco. Identificou-se que a tensão de soldagem apresenta um comportamento semelhante a uma onda senoidal e dependendo da inclinação da curva, seu sinal terá duas direções específicas, podendo ser uma inclinação positiva durante o crescimento da bolha ou uma inclinação negativa durante o crescimento da bolha. sua separação da área do arco de soldagem.

Nos experimentos realizados verificou-se que nos momentos em que a tensão diminui para valores inferiores a 5 Volts, não significa explicitamente que haja um curto-circuito, é simplesmente uma atenuação do arco.

Uma possível relação inversamente proporcional entre a voltagem média do experimento e a frequência (em bolhas por segundo (b/s)) também foi identificada. E, uma relação proporcional entre esta tensão e o diâmetro equivalente calculado. Além disso, é apresentada uma possível relação entre o coeficiente de variação da corrente e o do diâmetro das bolhas, porém, isso só poderia ser válido para os consumíveis e parâmetros de soldagem apresentados neste estudo.

A observação dos vídeos do experimento sugere que, diferentemente dos outros experimentos, durante a formação da bolha, o eletrodo básico, aglomerado com um aglomerante de polímero, adota uma aparência semelhante a flocos e se expande e se contrai em volume oscilando antes de se quebrar em vários pedaços menores. bolhas. Este fenômeno de bolha também foi observado mesmo sem a presença de curtos-circuitos ou quedas de tensão. Além disso, o aumento do diâmetro das bolhas desse eletrodo pode estar relacionado à presença de partículas de polímero no material adicional.

Com relação ao fenômeno da formação de bolhas no eletrodo revestido com fluxo de rutilo, percebeu-se um fenômeno mais suave de formação e desprendimento da bolha, o que pode estar relacionado à sua maior estabilidade nos parâmetros elétricos do processo.

Palavras chave: *Soldagem Submarina Molhada, SMAW, detecção visual em soldagem, fenômeno da bolha.*

ABSTRACT

The focus of this work is to analyze the dynamics of the bubbles resulting from the welding process, on the effect of different formulations of coated electrodes, in both polarities and varying the welding current. The visual analyses of the bubble formation have been accepted as a fundamental tool in studying the welding process due to its correlation effect with the process stability and so, the final weld bead. Also, the shielded metal arc welding process is still the dominant technique used in marine and submarine engineering due to its reasonable cost of implementation and suitable performance.

The proposed work includes the study of three different stick electrodes specifically designed for Underwater wet welding, including, two electrodes developed in the Robotics, Welding, and Simulation Laboratory, and a commercial one specific for underwater welding. The differences under direct and inverse polarity are highlighted by bubble evolution and arc stability analysis.

This work is developed through the use of a quality imaging system, a power supply, a data acquisition system, and a detection and tracking algorithm. The image processing algorithm identifies the bubbles generated in the shielded metal arc underwater welding experiments. Also, the algorithm facilitates the calculation of the projected area of the bubble and its equivalent diameter. Then, it is able to track the bubbles for monitoring purposes as well as to calculate their frequency.

As the imaging system and the signal are synchronized, it is possible to determine the relationship between the bubbles and the electrical characteristics of the arc. It was identified that the welding voltage presents a behavior similar to a sine wave and depending on the slope of the curve, its signal will have two specific directions, being able to be a positive slope during the growth of the bubble or a negative slope during its separation from the welding arc area.

In the experiments carried out it was found that in the moments in which the voltage decreases to values lower to 5 Volts, it does not explicitly mean that there is a short circuit, it is simply an attenuation of the arc.

A possible inversely proportional relationship between the mean voltage of the experiment and the frequency (in bubbles per second (b/s)) was also identified. And, a proportional relationship between this voltage and the calculated equivalent diameter. Also, there is a possible relationship is presented between the coefficient of variation of the current and that of the diameter of the bubbles, however, this could only be valid for the consumables and welding parameters presented in this study.

The observation of the experiment videos suggests that, unlike the other experiments, during the formation of the bubble, the basic electrode, agglomerated with a polymer binder, adopts a flakes-like appearance and it expands and contracts in volume oscillating before breaking into several smaller bubbles. This bubble phenomenon was also observed even without the presence of short circuits or voltage drops. Also, the increase in the diameter of the bubbles of this electrode could be related to the presence of polymer particles in the additional material.

With regard to the phenomenon of the bubble formation in the rutile flux coated electrode, a smoother phenomenon of formation and detachment of the bubble was perceived, which could be related to its greater stability in the electrical parameters of the process.

***Keywords**: SMAW, UWW, visual sensing in welding, bubble phenomenon.*

LIST OF FIGURES

Figure 1 - Diagram of the welding setup equipment used in all experiments (Adapted from the work in (URIBE et al., 2017)..... 18
Figure 2. Image pre-processing path to find the object of interest. 20
Figure 3 - A simplified scheme on the different bubble dynamic stages of a rutile-based electrode – 150A. a) Protective bubble. b) Detachment of the bubble. 20
Figure 4. Distance measure between frames. 21
Figure 5 - Monitoring proposed algorithm..... 22
Figure 6 - Relationship between bubble formation and welding voltage in a silicate oxidizer electrode with DCEN and 150A (section taken from a 2s video). 25
Figure 7 - Detachment of the bubble in a high voltage value (no arc quenching)..... 26
Figure 8 - Welding voltage oscillograms obtained from the Rutile based and the Basic with polymer electrodes during a single welding trial. (a) Rutile based electrode – 150 A – DCEN, (b) Rutile based electrode – 150 A – DCEP, (c) Basic with polymer electrode – 150 A – DCEN, (d) Basic with polymer electrode – 150 A – DCEP. 28
Figure 9 - No arc extinction in voltage values lower than 5V. 29
Figure 10 - Welding voltage values (considered normal condition values) without visual presence of the electric arc..... 30
Figure 11 - Relationship between voltage and frequency in bubbles per second (inversely proportional). 31
Figure 12 - Relationship between the average voltage and the average and maximum diameter of the bubble (directly proportional)..... 31
Figure 13- Relationship between the coefficient of variation of the process current and that of the diameter of the bubbles..... 32
Figure 14 - Bubble generation the tail of the welding puddle. 33
Figure 15 - The number of short circuits on each experiment..... 34
Figure 16 - Appearance of the electrode bubble (flakes) with addition of PTFE in direct polarity. 36
Figure 17 The time that the bubble is remining in the welding area (blue) and the diameter of the bubble (green). 38
Figure 18 - Histograms (Voltage x Current) of the different experiments. On the left the DCEN experiments and on the right the DCEP (same order as in figure 8). 39
Figure 19 - Oscillograms Voltage (left) and Current (right) of WW70 180A. In the upper part the data taken in DCEN polarity and in the lower part the data obtained in DCEP polarity..... 40
Figure 20 - Oscillograms Voltage (left) and Current (right) of WW70 150A. In the upper part, the data taken in DCEN polarity and in the lower part, the data obtained in DCEN polarity. 40
Figure 21 - Oscillograms Voltage (left) and Current (right) of Basic + PTFE 150A. In the upper part the data taken in DCEN polarity and in the lower part the data obtained in DCEP polarity..... 41
Figure 22 - Oscillograms Voltage (left) and Current (right) of Hydroweld FS 150A. In the upper part the data taken in DCEN polarity and in the lower part the data obtained in DCEP polarity. 41

LIST OF TABLES

Table 1 - Welding parameters. 18
Table 2 - Calculated average voltage and current values, their respective standard deviations and coefficient of variation. A, B and C correspond to the silicate oxidizer, basic with polymer and rutile-based electrodes respectively. 27

TABLE OF CONTENTS

1. INTRODUCTION 10
   1.1 Research objective 11
      1.1.1 Specific objectives 11
2. BACKGROUND 12
   2.1 Underwater Wet Welding 12
      2.1.1 General approach 12
      2.1.2 Study of the bubble formation phenomenon. 12
   2.2 Computer vision algorithms for image processing 14
3. EQUIPMENT AND METHODOLOGY 17
   3.1 Experiment and Materials 17
   3.2 Welding system 18
   3.3 Image capture system 19
      3.3.1 Image preprocessing 19
      3.3.2 Edge Contour Extraction. 19
      3.3.3 Calculation of the variables 19
4. RESULTS AND DISCUSSION 23
   4.1 Visual output from the algorithm 23
   4.2 Correlation between the bubble phenomenon and the welding voltage and current signals 23
   4.3 Attenuation in arc intensity at values less than 5V 27
   4.4 Visual 27
   4.5 Generation of a bubble adjacent to the melting pool. 32
   4.6 Comparison of all consumables at 150 A. 32
   4.7 150 A vs 180A on silicate oxidizer electrode. 34
   4.8 Basic electrode with addition of PTFE. 35
   4.9 Arc Stability Analysis. 37
5. CONCLUSIONS 42
6. Appendix A 52

1. INTRODUCTION

Underwater wet welding (UWW) has become a highly interesting topic of research in the last few years. This is because more machinery for extracting, transporting and storing gas and oil from marine resources have been generated with the increasing demand for these natural deposits by the population (CHEN et al., 2018; JIA et al., 2019a; ŁABANOWSKI, 2011; ROWE; LIU, 2001; YANG et al., 2019). Also, because its economical and procedure potential in comparison with the other welding techniques (CHEN et al., 2019; LI et al., 2018; WANG et al., 2018b, 2019b). Nowadays, a vast quantity of the ultimate improvements reported for underwater welding has been in the flux core arc welding process (FCAW) (MENDONÇA; BRACARENSE, 2019; WANG et al., 2018c, 2018a, 2019a, 2017; ZHANG et al., 2019). However, given the variety of techniques develop with Flux Cored Arc – underwater welding, shielded metal arc welding (SMAW) is still the dominant technique used in marine and submarine engineering (AMARAL; MORENO-URIBE; BRACARENSE, 2021; BERNARDI; GONÇALVES SILVA; SCHWEDERSKY, 2018; KLETT et al., 2020; RIBES VIVÓ, 2020; URIBE et al., 2017).

In the seek to enhance the performance and joining quality, the visual analyses of the bubble formation has been accepted as a fundamental tool in studying the welding process due to its correlation effect with the process stability and so, the final weld bead (DE ROSA OLIVEIRA, 2012; DE ROSA OLIVEIRA; SOARES; BRACARENSE, 2015; FENG et al., 2017; GUO et al., 2015; LIU et al., 2000; WANG et al., 2019b). That is why in recent years this tool has been incorporated to help researchers analyze the interaction of the bubble with the arc, the droplets and the surrounding water aiming to maintain the bubble protecting the weld pool and understand how else the weld join could be improved (FENG et al., 2017; JIA et al., 2016, 2019b; LI et al., 2020; WU et al., 2020; YANG et al., 2020). However, despite the technological advances of computer science in images analysis and data processing, only few researchers have relied on these resources to better calculate and process the data generated (CHEN; FENG, 2014; CHEN; JIA; FENG, 2013a, 2013b; ORTIZ et al., 2021; WANG et al., 2019b).

Nonetheless, the visual sensing analysis has helped to identify how new proposed variances in the manufacturing underwater welding process could achieve better quality for the joint. Chen et al. (2019) used images (X-ray) to study droplet transfer and the bubble behaviors using gas-shield cover. As the bubble stayed for a longer period of time, the weld reinforcement showed better and smoother appearance than that of traditional wet weld. They also mentioned that the

water dissociation when shielding gas is not provided induced to hydrogen pore defects. Later, CHEN et al. (2020) mentioned a significant decrease in volume of the protecting bubble with the incorporation of an ultrasonic wave, however, this methodology allows the gas releasing and escaping from the melt pool. They reported porosity and hydrogen diffusible content decreases of 0.5% and 18.6 ml/100 g, respectively, with an ultrasonic power of 720 W. Lastly, CHEN et al. (2020a) used X-ray imaging to detect variances in the molten drop while applying hydrostatic pressure. Their study showed that the diffusible hydrogen content and the porosity in the weld metal, tend to increase when increasing the water deep.

In this way, the focus of this work is to analyze the dynamics of the bubbles resulting from the welding process, and the effect of different formulations of coated electrodes, in both polarities and varying the welding current. This work is developed through the use of a quality imaging system, a power supply and a data acquisition system. This document focuses on the use of an image processing algorithm to identify the bubbles generated in the shielded metal arc underwater welding (SMA-UW) experiments. The algorithm facilitates the calculation of the projected area of the bubble and its equivalent diameter. Then, it is able to track the bubbles for monitoring purposes as well as to calculate the frequency of them.

The extracted data from the images is used for a better understanding of the behavior of the SMAW-UW process. That is why, the possible correlation of these variables with the variables that represent the characteristics of the electric arc, like the welding voltage and the welding current, is discussed. to report the findings about the phenomena observed in welding in an aqueous environment.

The proposed work includes the study of three different stick electrodes specifically design for UWW, including, two electrodes developed in the Robotics, Welding, and Simulation Laboratory (LRSS), and a commercial one specific for underwater welding. The differences under direct and inverse polarity are highlighted by bubble evolution and arc stability analysis.

1.1 Research objective

Develop an algorithm for the detection of bubbles in underwater wet welding.

1.1.1 Specific objectives

- Detect a reasonable approach for the detection of images in SMA-UW
- Analyze the new visual variables with the conventional for SMA-UW

2. BACKGROUND

2.1 Underwater Wet Welding

2.1.1 General approach

Underwater wet welding has its application in offshore structures for extraction and distribution of oil and gas and for green energy generators such as wind turbines or those submerged in the sea. This technology is also being used in the construction and maintenance of nuclear plants. This work focuses on wet underwater welding, since it is the category that is being used the most at the moment, due to its ease of execution, especially for preventive maintenance.

Although the main process used in practice is the SMAW, worldwide efforts have been focusing on improving the FCAW process due to the benefits it brings in terms of time, quality and procedures cost, this last one is significant in large projects. FCAW uses power sources of constant voltage in which the welding parameters used are different, for example, the diameter of the wire. However, some of the principles that govern SMAW are maintained in FCAW because the technology of the electric arc is the same. What it changes is the characteristics of the process. This allows findings in either of the two processes to contribute to the improvement in the quality of the underwater wet welding.

One of the greatest discoveries in the field in the last decade was the complex connection that the bubbles generated in this welding process share with the electrical parameters and how a better understanding of this phenomenon can lead to an improvement in the quality of the weld bead.

2.1.2 Study of the bubble formation phenomenon.

2.1.2.1 International

Since MASUBUCHI AND TSAI (1977) with their mathematical model to predict bubble growth as an ideal gas, attempts have been made to discover how bubble interaction can decrease welding collateral effects in an aqueous environment. However, JIA et al. (2016), in their experiment with the FCAW process, presented images of a quality that allowed a better visualization of the bubble phenomenon. In their work it is concluded that the bubbles grow in a pulsed manner with variable speed instead of continuously and smoothly. Also, they

mentioned how the visual study of the process allows to see that the bubble also affects the drops of molten material, the welding arc and the high-temperature welding pool.

Another outstanding work on the analysis of the bubble phenomenon was presented by FENG et al. (2017) where they reported that performing tests with a higher feed rate (and, consequently, higher welding current) for the tubular wire process in a humid environment, the bubbles increase in size and decrease in frequency. In their document, they conclude that the occurrence of bursts or collapses of the bubble occurs erratically, which affects the stability of the process. Finally, they also discover four different modes of bubble evolution that can be divided according to the behavior of the bubble during its evolution along with the characteristic of the arc in the welding process. In the first and fourth modes, the generated bubbles do not have enough volume to protect the arc and their volume is so large that the bubble bursts, leaving the arc unprotected given its low and high current, respectively. In the second mode, arc extinction does not occur, however, the oscillation of the signal is considerable and, as described by the authors, in the third mode of evolution, the bubble floats smoothly and arc extinction cannot be observed, which reflects the ideal stability of the welding arc.

2.1.2.2 National

The Laboratory of Robotics Welding and Simulation (LRSS) of the Federal University of Minas Gerais, even with its strong lines in fatigue analysis and the development of consumables for welding, has developed important contributions in terms of the visual analysis of the bubbles generated in the underwater welding process. In the investigations of DE ROSA OLIVEIRA (2012) and DE ROSA OLIVEIRA et al. (2015) found a correlation between the bubble formation and separation and the electrical signals using coated electrodes. With the limitations of the visual sensors by that time (high speed camera resolution), they found that the intensity of the arc decreased at the moment that the bubble was absent from the area of the electric arc (detachment). Then, this intensity increased automatically with the beginning of the formation of a new bubble. In this publication, the frequency of the bubbles was calculated for different electrodes and a possible relationship between this magnitude and the number of events in which the current signal decreased to values 5% lower than the average current was highlighted.

In 2019, MENDOZA AND BRACARENSE (2019) carried out a study of the phenomenon for self-protected tubular wire. Their main results were how variables such as a proposed dry contact tube and increased feed rate increased bubble diameter and process stability. The

document highlights the vital importance of understanding the dynamics of bubble formation to improve the stability of the electric arc.

A paper on applications of computer vision techniques for contour detection in underwater welding was recently published (ORTIZ et al., 2021). The advances documented in this disclosure are the basis for the results obtained in this document.

Other outstanding studies in Brazil are presented at the Institute of Mechatronics Welding - LABSOLDA of the Federal University of Santa Catarina. BERNARDI et al. (2018) in his studies of an arc voltage control for coated electrodes states that the higher the welding current, the greater the arc stability and the greater the average diameter of the bubbles. He mentions that this is related to a higher rate of fusion of the consumable and greater repeatability of the experiments. This tendency remains undifferentiated with the polarity of the welding current.

2.2 Computer vision algorithms for image processing

Among the researchers who have implemented image processing techniques in the welding process, GOMES et al. (2002) developed a computer program to quantitatively analyze the acquired images of droplet transfer modes in MIG/MAG welding. In addition to the possibility of analyzing a large number of samples, the Vídeo-analisador (Video Analyzer in English), as it is called by the authors, presents time savings of 60 times with greater accuracy of the results when compared with manual measurement on the same images. Also, the methodology use in this study (digital image processing) did not make approximations in the geometry of the droplet as the projected area was used to calculate the diameter.

The study demonstrated that measurements that depend on the user's experience and visual acuity are more prone to errors and the repeatability of the results becomes difficult. This corresponds with other studies which mention that methods by hand use approximations in metrology (BERNARDI; GONÇALVES SILVA; SCHWEDERSKY, 2018; MENDONÇA; BRACARENSE, 2019).

RESENDE (2013) conducted a study of operational characteristics of the PLASMA-MIG process, where it states that knowing the diameter of the droplet (consequently the mass) and its speed when it collides with the weld pool, it is possible to determine the amount of effective movement applied on the base material. He attributes this term as the main dynamic feature of the droplet that can influence the formation of the weld bead. The author calculates the mean

diameter, the output speed of the electrode and the speed when reaching the weld pool, the mean acceleration, the arc length, and the position of each droplet using digital image processing (DE ARAUJO; VILARINHO; ALVES DE RESENDE, 2011). Among the main conclusions, he emphasized that the increase in current in the arc tends to increase the rate of arrival of the drops in the weld pool.

Also, GIRÓN CRUZ (2019) developed a methodology for monitoring metal transfer using image processing techniques algorithms developed with MATLAB 12a software tools. The author mentions that the variable manipulated to determine the size of the droplet was the largest horizontal row (in pixels) of the projected area, for which it was necessary to assume the geometric volume of each drop as a sphere.

These investigations had been made with a technique image called shadowgraphy. However, the while (DE ARAUJO et al. (2011) used the projected area to calculate the equivalent diameter of the object of interest, GIRÓN CRUZ (2019) selected the largest horizontal row of the projected area as the diameter of the drop.

After detecting the size of the object, it could be estimating their centroid. And, and with a record of the position of each object (centroid), the developer could track different objects as the same time. To determine the detachment frequency and diameter of the droplets, the algorithms proposed by DE ARAUJO et al. (2011) was used. And, to track and monitor the different objects from frame-to-frame STURDEVANT; HOLLINGER; CHITIVELI (2020) provide a code pattern for processing the frames of a video using a Jupyter Notebook, OpenCV, and IBM Maximo Visual Inspection.

Until now, the computer vision methodologies presented have application in a dry environment. However, WANG et al. (2019b) used image processing techniques to calculated and determinate the geometries of the bubble. Also, they presented three distinct stages as a function of the heat input. The authors emphasize that detecting bubble growth provides a new direction for the development of underwater wet welding technology. And, they conclude that a larger heat input provides a large possibility for a better protective effect and a larger weld penetration.

Present day, among the best-known tools for computer vision are OpenCV (Open-Source Computer Vision Library) and the MathWorks Computer Vision Toolbox (MATLAB, 2010) They basically differ in that OpenCV is used within the libraries used by MATLAB and in addition the Computer Vision Toolbox has algorithms that are not found in OpenCV in its own code (M code). On the other hand, the MathWorks software is not free. The MATLAB license

is 275 USD and the Computer Vision Toolbox license is 110 USD, both values are for one year (values for students).

Another difference between the two tools is that OpenCV allows different programming languages in the use of its library, such as python, java, C/C++, .Net and others, while MATLAB has only been extended to C/C++ so far. However, since both libraries are widely used, interfaces have been developed that allow the interaction of both tools and facilitate their use without the obligation to learn a new programming language. These interfaces continue to be actively developed at this time (BRADISKI, 2000).

3. EQUIPMENT AND METHODOLOGY

3.1 Experiment and Materials

The proposed work includes the study of three different stick electrodes specifically design for UWW. The electrodes developed in the Robotics, Welding, and Simulation Laboratory (LRSS) are, a silicate oxidizer based on Fe_2O_3/TiO_2 and the other electrode is $CaF_2/CaCO_3$ (basic) agglomerated with a polymer binder. The third included electrode is a commercial one and specific for underwater welding composed with a rutile base.

For the experiments, a gravity welding system was used, as shown in the Fig. 1, where the drag welding technique was applied. The angles configured for the mechanized process were α=60° and β=100° according to values reported in the literature (ANDRADE et al., 2010; ARIAS; BRACARENSE, 2017; BRACARENSE et al., 2010; DE ROSA OLIVEIRA, 2012; DE ROSA OLIVEIRA; SOARES; BRACARENSE, 2015; MENEZES; PESSOA; BRACARENSE, 2019; MORENO-URIBE, 2018; URIBE et al., 2017). For each of the eight experiments, a combination of different welding parameters was established (Table 1). For the silicate oxidizer, basic with polymer and Rutile based electrodes a welding current of 150A were set. However, with the silicate oxidizer electrode a second current level of 180A was added for comparative purposes. Each combination of parameters was executed on both polarities (DCEP & DCEN). All experiments were carried out in tap water, in an aquarium intended for underwater welding operations. Visual and electrical signals were collected simultaneously. During the welding process, due to the fact that the high-speed camera remained stationary in relation to the welding zone, the videos were filmed 10 seconds after the start of the process ensuring an almost stable regimen.

The voltage and the welding current data for each condition were acquired at a frequency of 5kHz. The data referring to average welding current, the average welding voltage and their respective standard deviations were calculated using the Sinal software (AMARAL; MORENO-URIBE; BRACARENSE, 2021; ROSAS; MODENESI; ORTIZ, 2020; SANTANA; MODENESI, 2011; URIBE et al., 2017; VAZ; BRACARENSE, 2015). Electric arc power, resistance, short circuit percentage and number of short circuits were also calculated in a 7-second period and in the video period (2 sec).

Figure 1 - Diagram of the welding setup equipment used in all experiments (Adapted from the work in (URIBE et al., 2017).

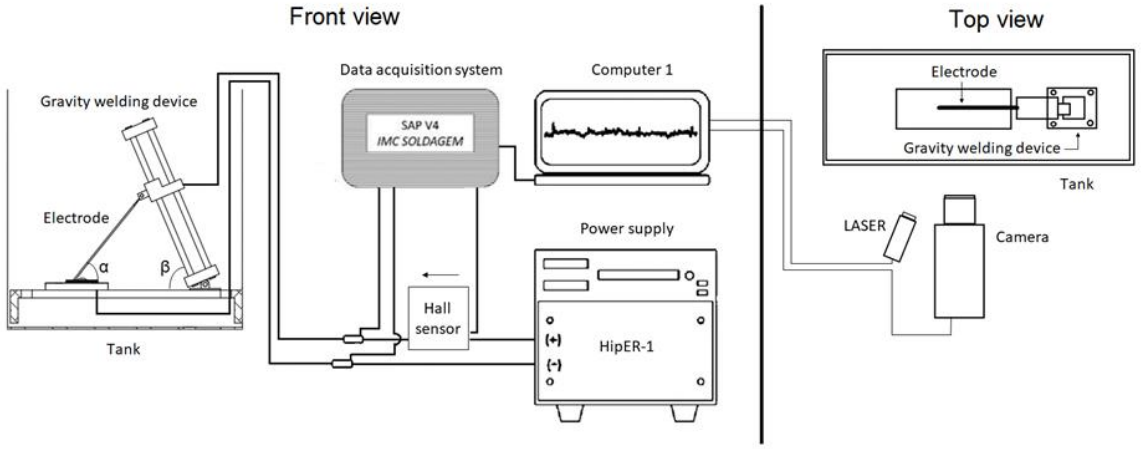

Table 1 - Welding parameters.

Consumable	Welding current (A)		Polarity	
	150	180	DCEN	DCEP
silicate oxidizer	*	*	*	*
Basic with polymer	*		*	*
Rutile based	*		*	*

*The welding current values are presently used in the LRSS-UFMG and reflect the best behavior of these consumables under the conditions of this study (A. Q. BRACARENSER. LACERDA DE SOUZAM. C. M. DE SOUZA COSTAP. E. FARIAS. LIU, 2002; BRACARENSE; LIU, 1993; MENEZES; PESSOA; BRACARENSE, 2019; PESSOA et al., 2006; QUINN; BRACARENSE; LIU, 1997).

3.2 Welding system

For the welding process, the simulated depth was 0.4 m, and was used an IMC Hip-ER 1 DC power source for welding operations in sub-marine environment with coated electrode. In addition, it was used a SapV4 data acquisition equipment from IMC company, with current measurement ranges of up to ±600A with a resolution of 0.8A and a voltage measurement of up to ±100V with a resolution of 1V and a maximum error of 1% (SOLDAGEM BMI, 2022). Bead-on-plate welds were manufactured using ASTM A-36 carbon steel with 1/4 inch of thickness. The different coated electrodes used have a nominal diameter of 3.25 mm.

3.3 Image capture system

The imaging system was developed based on a high-speed camera (Motion Pro Y4-S2 of the company IDT) and a LASER system (CAVILUX HF of CAVITAR) with a filter 640 nm (visible), with a frequency of 1000 fps and a resolution of 1016 × 1304.

3.3.1 Image preprocessing

Each video was split into images (frames) to be later processed. As shown in the Fig. 2, after the filtering, the images were processed with the adaptive threshold (mean) to detect the contours of the bubbles. Step followed by a dilation to close some contours not properly detected by the variation of light in different parts of the image. Subsequently, we proceeded to perform the imfill function that consists of filling these contours (KALAKUNTLA; ANDRIAMANALIMANANA, 2021). Then, objects considered as noise in the image were removed through erosion. Finally, depending on the section of the video, both the shadow cast by the electrode on the background of the screen and the electrode itself were removed. The above methodology is justified in facilitating the correct detection of the contours of the bubbles, especially when there are shadows behind these bubbles.

3.3.2 Edge Contour Extraction.

Consequently, the contour detection was performed with the findContours tool, available in the OpenCV library, and the detected areas smaller than 45000 pixels were disregarded. With the remaining contours, the area and the centroid of the detected contour were calculated. After the geometric measurements, the contours were listed and monitored as they appeared within the video and, for each contour, the number of the frame, the centroid and the area of each bubble were recorded (Fig. 3).

3.3.3 Calculation of the variables

To identify whether the registered object is in a new image (tracking), an identification algorithm was defined (Fig. 5). The follow-up variables were simplified to hyper-parameters such as the size and distance as used by (ORTIZ et al., 2021). For the algorithm, a maximum allowable distance between one frame and another was defined (Fig. 4). In this way, the distance between each of the centroids of the monitored objects with the objects in the new image is calculated. If the distance between the monitored object and the nearest detected new object

was less than the predefined distance, it was considered which was the same object. If this condition was not met, it was perceived as an undefined object and registered in a new temporary matrix (No_defined) where it is related which of the registered objects is closest to it, in what position within the list of objects of the new image it is located, the distance between these two objects, the position and its area.

Figure 2. Image pre-processing path to find the object of interest.

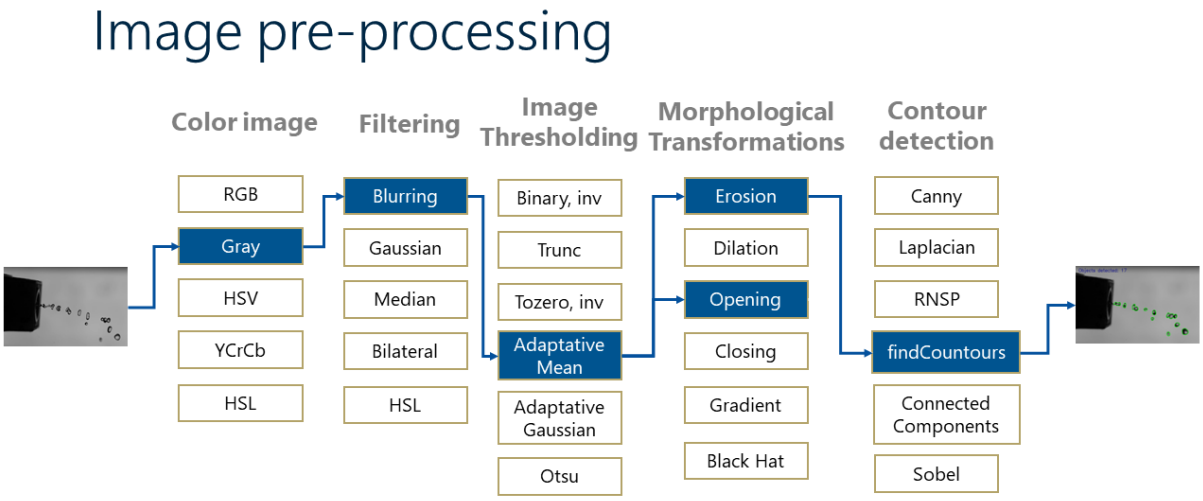

Figure 3 - A simplified scheme on the different bubble dynamic stages of a rutile-based electrode – 150A. a) Protective bubble. b) Detachment of the bubble.

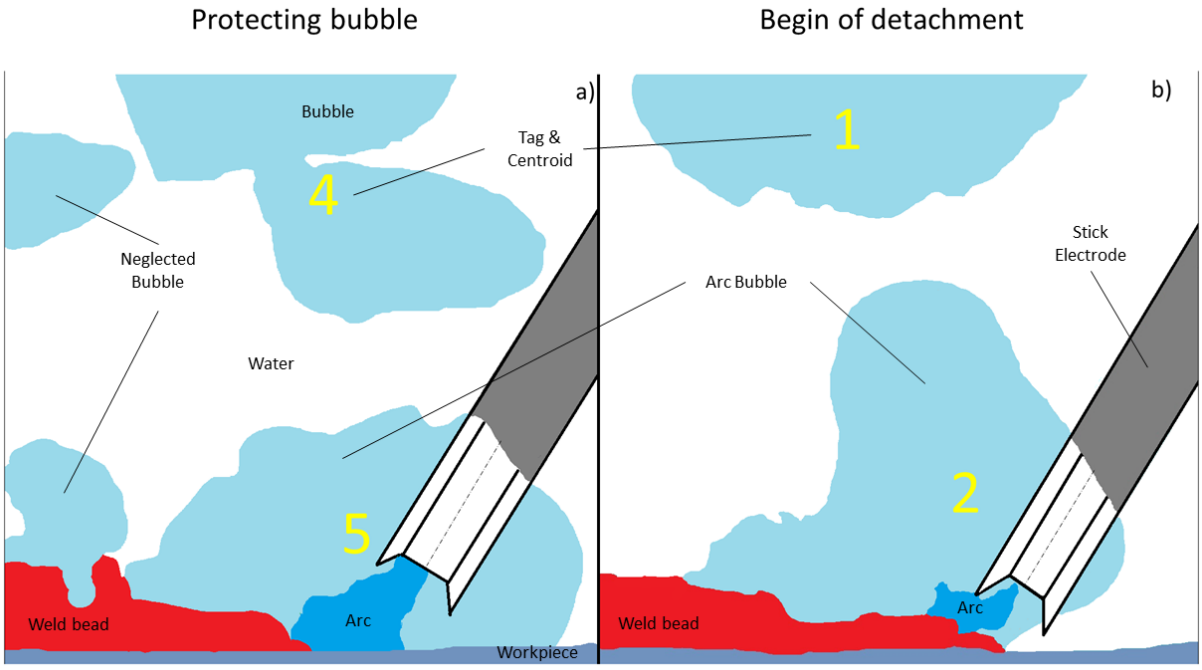

Once the previous process for all new objects was completed and the No_defined matrix was demarcated, a decision was made on the classification of those objects depending on the number of elements in the array. That is, if this temporary matrix only had one element, the following logic will be taken into account, if the number of objects detected in frame n is less than the amount in frame $n-1$, the label will be assigned to the nearest object of the previous frame, but if the number of objects in the two frames are the same or the number of objects of frame n is greater, it is identified as a new object and the algorithm proceeds to create a new label for later monitoring.

If there is more than one object within No_defined, the first thing that is identified is whether more than one new object relates to the same registered object. Objects that meet this condition are registered in another temporary array named Solitaires, and for each of the remaining objects a new tag is created.

Finally, for the objects registered in the Solitaires array which relate to the same registered object, the object with the largest projected area is assigned as an update of the position and area of the monitored object (to which it came closer) and for each of the remaining ones a new label is created. It is important to clarify that, although this last condition worked for most of the videos in this experiment, it was observed that the condition that states that, in a separation of the bubble, the bubble with the largest projected area will retain the label varied to the one with the smaller area doing so (it will retain the label) to monitor the bubbles according to reality. That is, in most cases while the detachment bubble stage, the bubble that stood out from the welding pool was greater than the one kept there, however, it was also presented, although rarely, that the bubble that stood out was smaller than the one that was kept protecting the welding arc and the molten material.

Figure 4. Distance measure between frames.

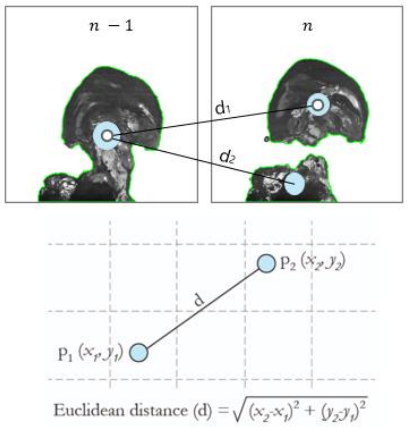

Figure 5 - Monitoring proposed algorithm.

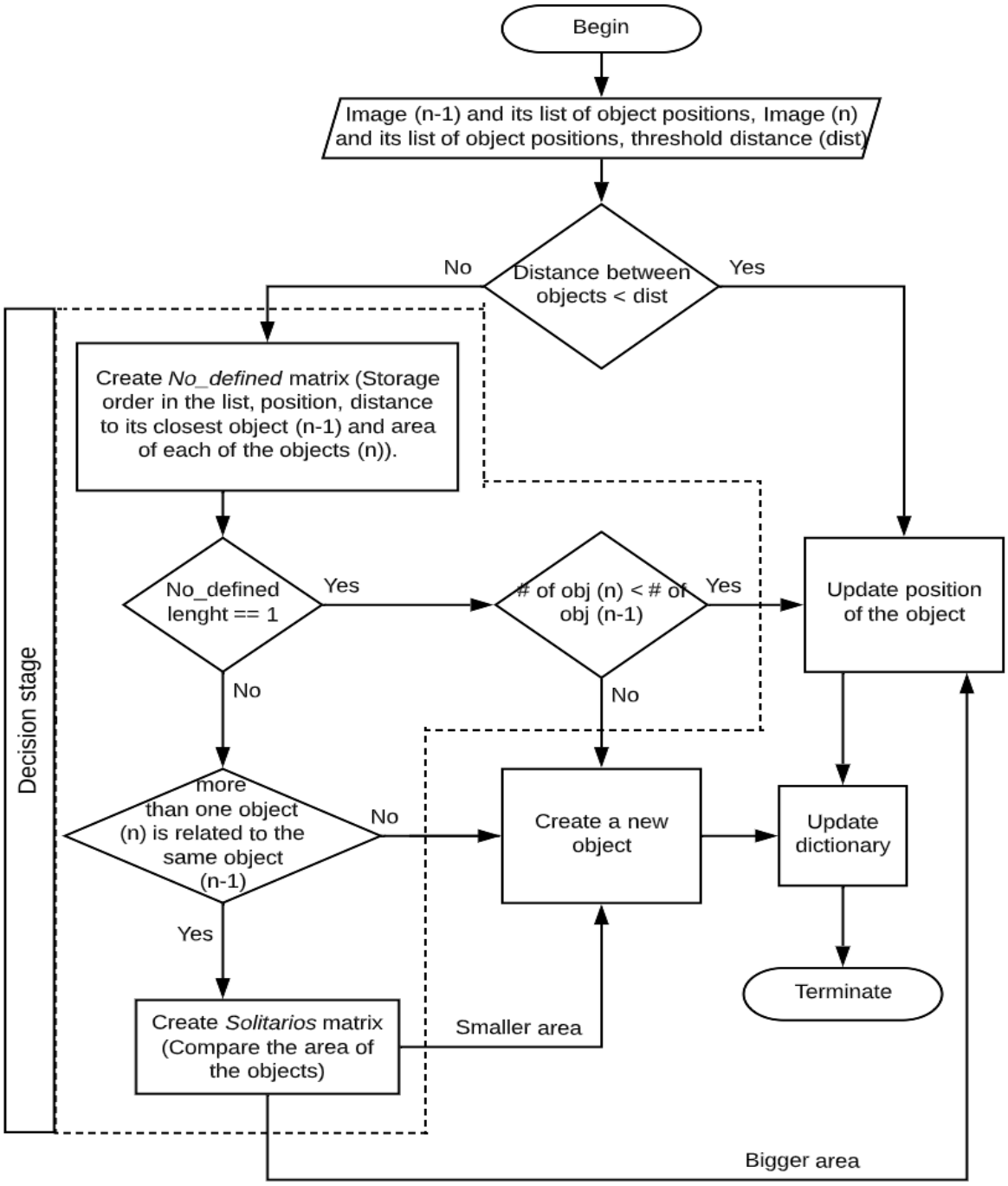

The data taken from the monitored elements was saved in a python dictionary and later converted into a DataFrame to facilitate the generation of graphs. With the frame number of each bubble and the frequency of the camera, the frequency of bubbles per second was calculated. With the values of the areas, the equivalent diameter was calculated by assuming the bubbles as circular. As a comparison measure, the average diameter and maximum diameter of each bubble were determined.

4. RESULTS AND DISCUSSION

4.1 Visual output from the algorithm

The results generated by the algorithm allowed the detection and tracking of the droplets (video 1, video 2, as well as they could support to an understanding of the interaction between them. The study by calculating the projected area and the centroid of this area facilitated their tracking and the study of motion in more than one dimension.

The video 1 is a silicate oxidizer electrode DCEP with a current od 150A and for the video 2 used the same parameter except for a current of 180A. Both videos have the contours of the bubbles shown in green, their tag or number identification in Yellow, where the number is in the same position where the centroid of each contour is. Also, as the algorithm is tracking the objects, it displays the number of objects detected in red. All colors were chosen to be distinguishable from the other information between the images. For a better appreciation of the bubble phenomenon, the videos are in 5 fps.

4.2 Correlation between the bubble phenomenon and the welding voltage and current signals

In the visual inspection to the videos of the welding process, it was observed that the phenomenon of generation and detachment of the bubble is continuous, but, a defined frequency (random) is not perceived as revealed in the literature (DE ROSA OLIVEIRA; SOARES; BRACARENSE, 2015; JIA et al., 2016; MENDONÇA; BRACARENSE, 2019; WANG et al., 2018c, 2018a). However, it has been identified that the phenomenon of bubble formation and the voltage values are correlated and they can therefore affect each other (DE ROSA OLIVEIRA; SOARES; BRACARENSE, 2015; WANG et al., 2018b; YANG et al., 2020; ZHANG et al., 2019). Similarly, the phenomenon of formation and detachment of bubbles depends on other variables such as gas reactions (WANG et al., 2018a), the pressure within it (JIA et al., 2016), and the thrust force (buoyancy) (WANG et al., 2019b).

As the imaging system and the signal are synchronized, it is possible to determine the relationship between the bubbles and the electrical characteristics of the arc. It was identified that the welding voltage presents a behavior similar to a sine wave and depending on the slope of the curve will have two specific directions, being able to be a positive slope during the growth of the bubble (Fig. 6 frame 312-375) or a negative slope during its separation from the welding

arc area (Fig. 6 frame 391-471). The voltage drops are related to the slowdown in the growth of the bubble or to the beginning of the detachment of it. Similarly, the increase in the voltage is related to the presence or growth of the protective bubble around the arc. In Fig. 6, the growth of the protective bubble of the electric arc and the increase in voltage from frame 312 to 375 can be seen. In frame 391, it can be perceived how the bubble has begun to detach at the sides and how that is related to a decrease in tension. This trend continues until frame 471, where, the bubble has completely detached from the welding surface and as a consequence there is a drop in the voltage. Then, the continuous phenomenon will form a new bubble.

Due to the oscillations of voltage during the bubble phenomenon, either in the stage of growth or detachment, the separation of it does not always occur at the end of the period identified in the form of the signal (i.e., Fig. 6 frame 471). In addition to the major sine wave seen (maxima and minima in the voltage signal), there are times when, within the slopes of these peaks and valleys, detachments of the bubble occurred (Fig. 7), when this happens the detached volume is partial and the arc is kept protected, that is, the arc is not extinguished.

Figure 7, illustrates an example of this phenomena. In the experiment 180A DCEP (silicate oxidizer), the detachment noticed in frame 515 is related with a volage of around 31 V, when this behavior is expected in values around 28V for this welding conditions.

Another fact identified is that the behavior of the operating voltage (maximum and minimum) is related to the average operating voltage of the consumables. In the case of the Basic with polymer electrode (150 A) the valley and peak values for direct polarity are 33.7V and 45.6V respectively, which are higher compared to the same polarity in the silicate oxidizer electrode at a current of 150 A, in which its values are for the valley and the peak are 22.3V and 27V (Fig. 6). The results for the positive electrode with polymer addition and the negative of the Rutile flux coated electrode are practically the same with an operating voltage of 31V (peak) and attenuations less than 10V (valley) (Fig. 8). Since the nominal diameters of the electrodes are the same, the variations in the working voltage values on the different electrodes used in the experiment are due to the type of electrode (the nature of the elements constituting the coating).

Figure 6 - Relationship between bubble formation and welding voltage in a silicate oxidizer electrode with DCEN and 150A (section taken from a 2s video).

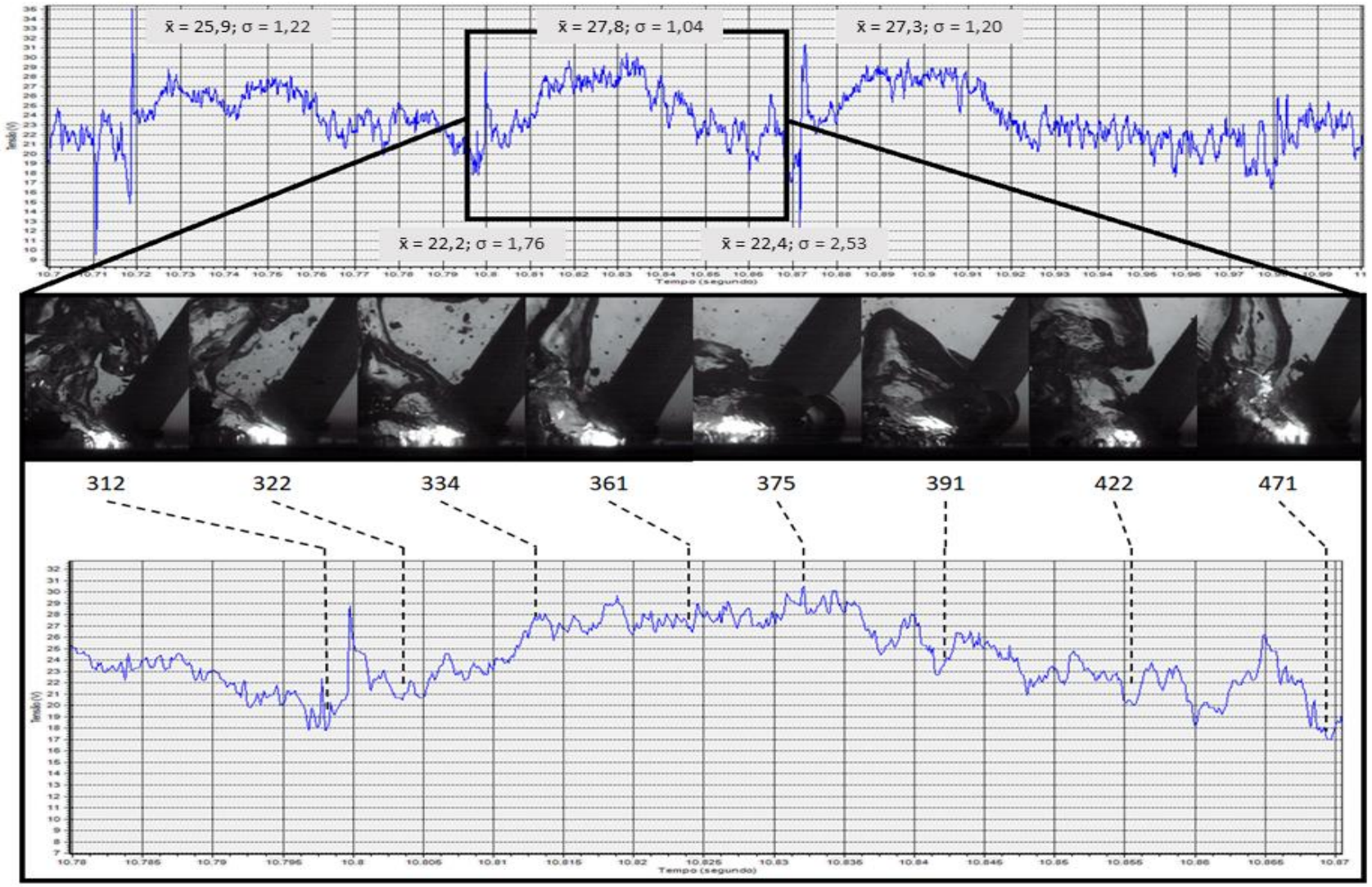

Figure 7 - Detachment of the bubble in a high voltage value (no arc quenching).

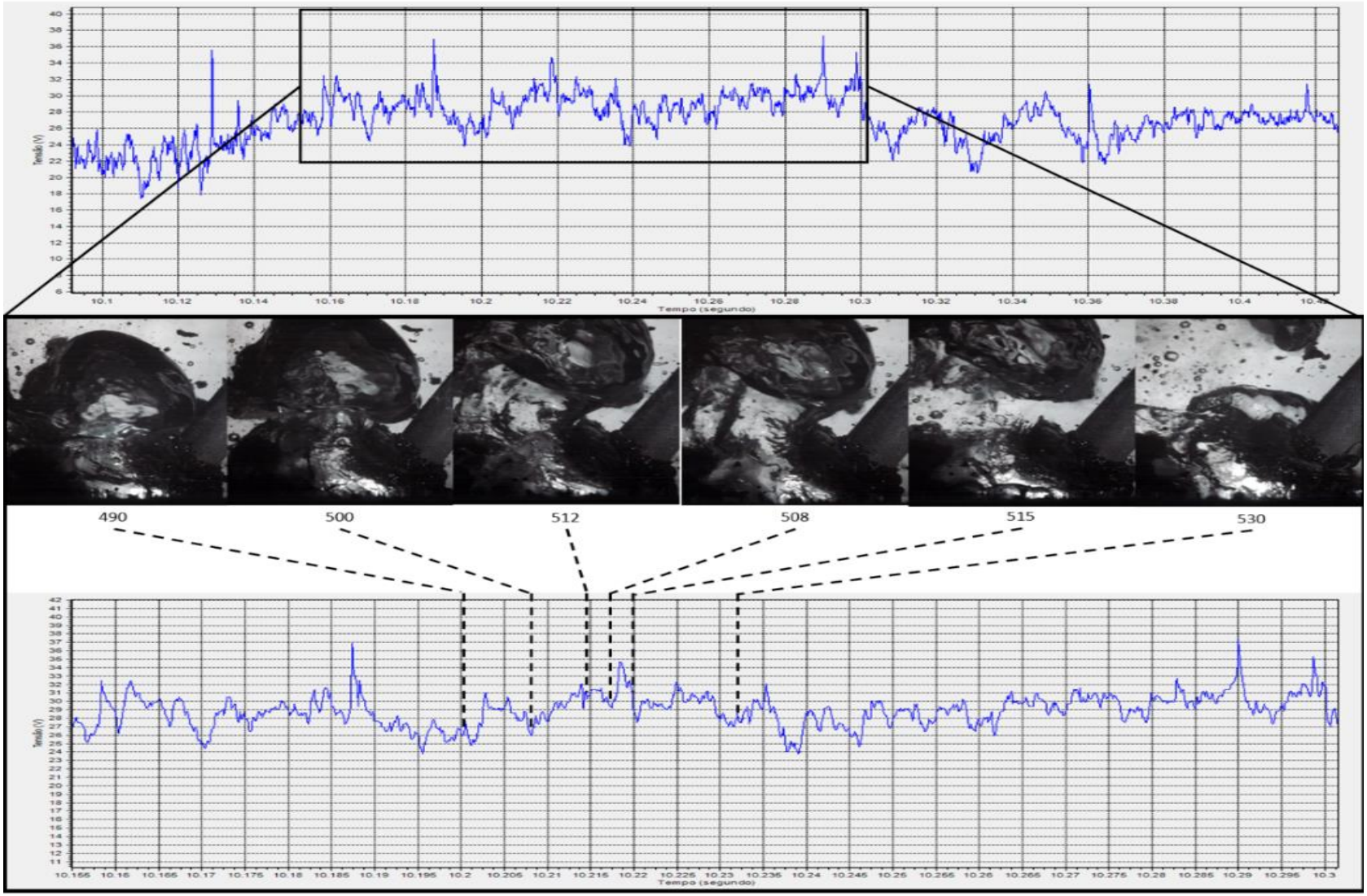

Table 2 - Calculated average voltage and current values, their respective standard deviations and coefficient of variation. A, B and C correspond to the silicate oxidizer, basic with polymer and rutile-based electrodes respectively.

		Data		Video*				cv (%)	
electrode	**polarity**	**voltage**	**Std**	**voltage**	**Std**	**current**	**Std**	**Current**	**Voltage***
A_150	-	22.5	3.1	22.45	3.01	150.2	3.7	24.43	13.38
A_150	+	23.8	2.4	23.30	2.42	149.5	3.6	24.30	10.39
A_180	-	27.4	2.6	26.98	2.18	179.6	3.8	21.33	8.073
A_180	+	25.9	2.4	27.00	2.5	178.2	3.8	21.08	9.26
B_150	-	35.2	6.6	34.53	6.53	149.4	5.1	34.12	18.89
B_150	+	28.7	5.5	27.93	5.39	151.4	4.0	26.24	19.30
C_150	-	32.5	3.4	30.81	2.79	149.5	3.8	25.60	9.06
C_150	+	35.8	3.1	34.93	2.88	150.9	3.8	24.91	8.23

*The column “Data” (7s) is the result of the analysis of the data thrown by the SapV4 equipment. Whereas, the Video columns (*) show the average and the standard deviation for the video time. And, the cv (%).

4.3 Attenuation in arc intensity at values less than 5V

For the underwater welding research community is common to consider voltage values equal to or less than that 5V as short-circuit (ESMERIO MAZZAFERRO, 1998; LIU et al., 2010; MORENO-URIBE, 2018). However, in the experiments carried out it was found that in the moments in which the voltage decreases to values lower to 5 Volts, it does not explicitly mean that there is a short circuit (Fig. 9), it is simply an attenuation of the arc (starting from which short circuit means that there is no arc). Due to the correlation of filming, signal acquisition and computer vision techniques, it can be seen that the voltage drops and works together with the detachment of the bubble, but there is not an effective short circuit, the arc does not go off.

4.4 Visual

Relating to the calculated data with the images of the different tests, it was observed that in the experiment with the silicate oxidizer electrode, at 150 A in DCEP, the voltage values in the valleys are higher than in the direct polarity and these are lower than 16V (Fig. 10). So, it can be assumed that the transfer of material is not by short-circuit, but the behavior of the arc (oscillating in a sinusoidal form) reflects the dynamics of the bubbles.

With regard to the phenomenon of the bubble formation in the Rutile flux coated electrode, a smoother phenomenon of formation and detachment of the bubble was perceived, which it could be related to its greater stability in the electrical parameters of the process (Video 3).

Figure 8 - Welding voltage oscillograms obtained from the Rutile based and the Basic with polymer electrodes during a single welding trial. (a) Rutile based electrode – 150 A – DCEN, (b) Rutile based electrode – 150 A – DCEP, (c) Basic with polymer electrode – 150 A – DCEN, (d) Basic with polymer electrode – 150 A – DCEP.

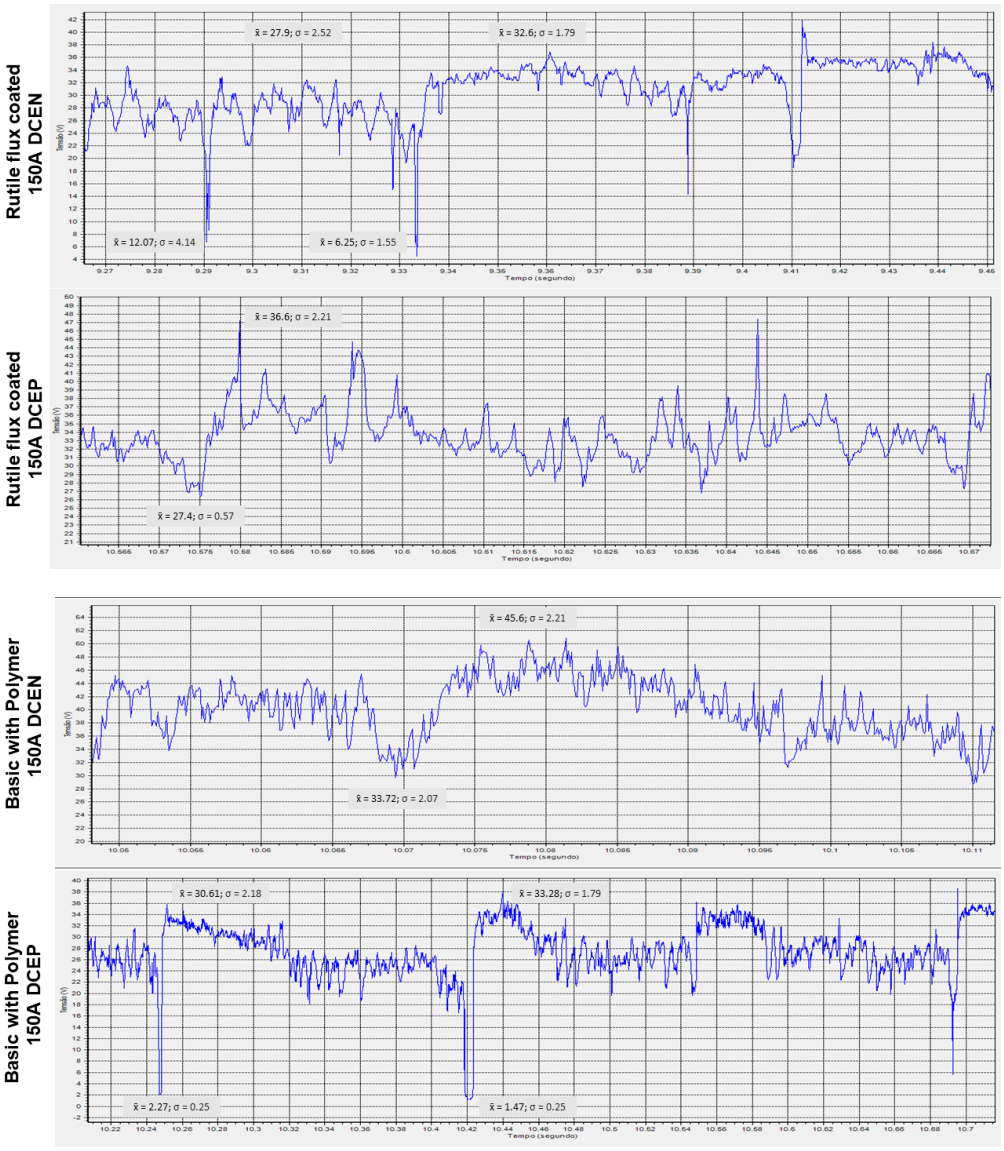

By correlating all the results, it was identified that the video time (2 s) data and the 7-second have a very similar behavior in the average voltage and the number of short circuits (Table 2; Fig. 15). A possible inversely proportional relationship between the mean voltage and the frequency (in bubbles per second (b/s)) was also identified, as shown in Fig. 11. However, Fig.

12 shows a proportional relationship between the voltage and the calculated equivalent diameter.

In order to compare the experiment with the analyses carried out in the literature, the coefficient of variation of according to (DE ROSA OLIVEIRA; SOARES; BRACARENSE, 2015) was calculated (Table 2). In Fig. 13, a possible relationship is presented between the coefficient of variation of the current and that of the diameter of the bubbles, however, this could only be valid for the consumables and welding parameters presented in this study.

Figure 9 - No arc extinction in voltage values lower than 5V.

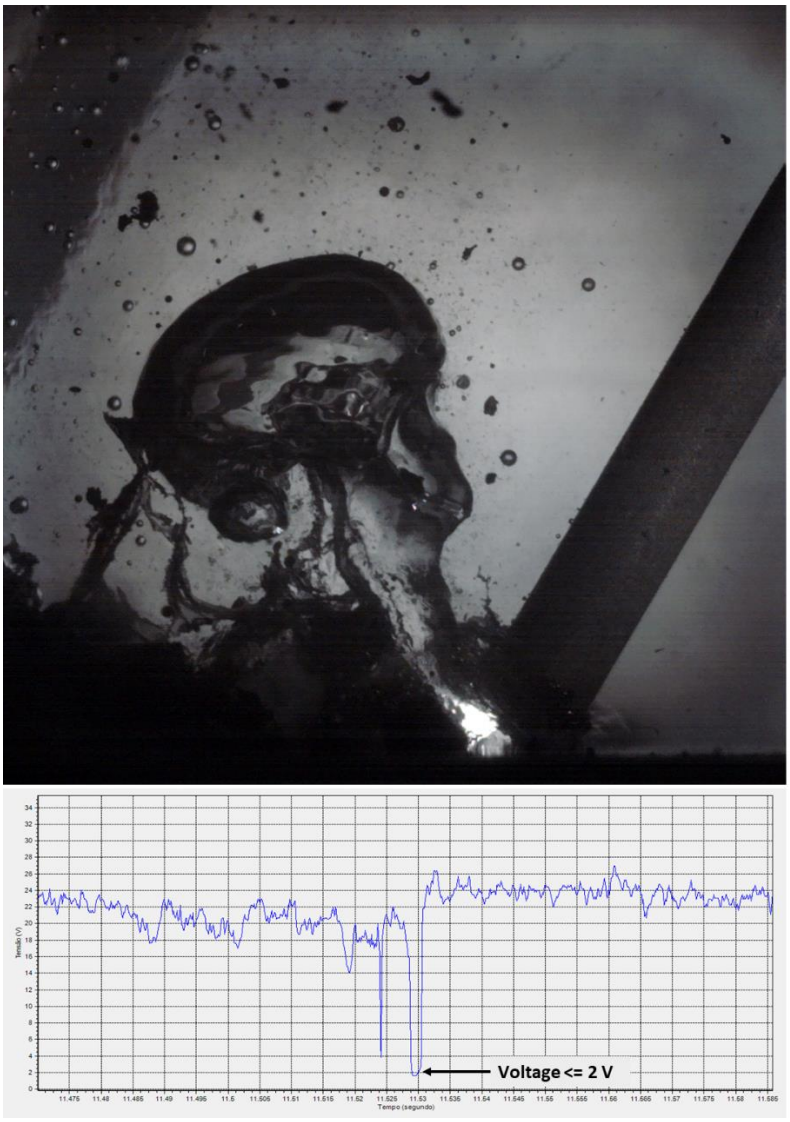

Figure 10 - Welding voltage values (considered normal condition values) without visual presence of the electric arc.

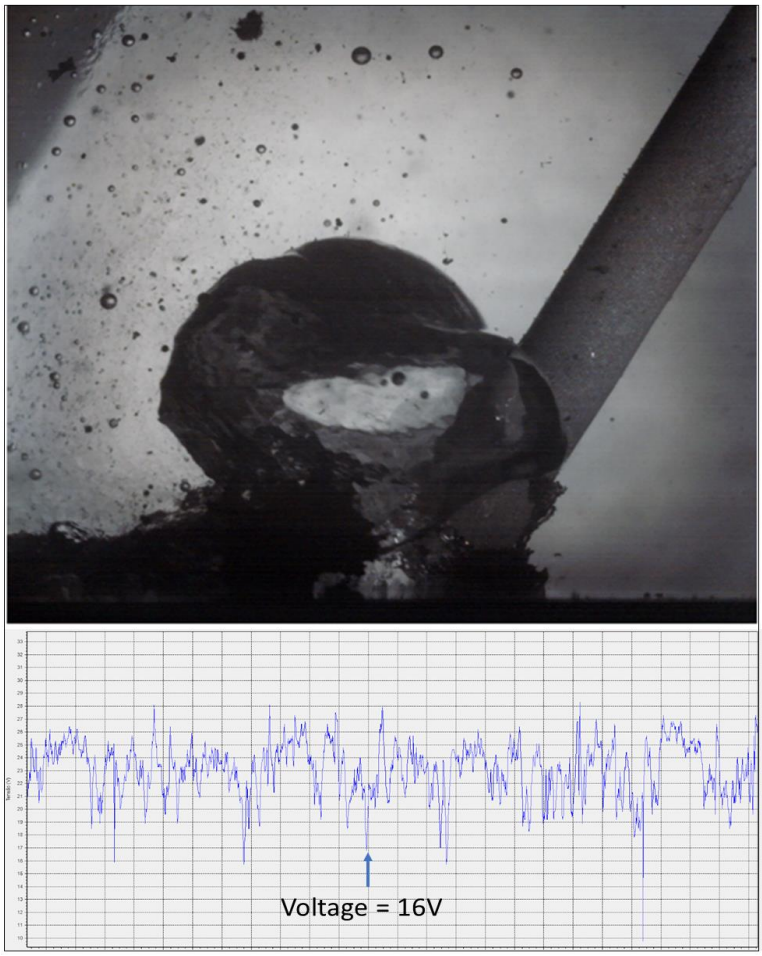

Figure 11 - Relationship between voltage and frequency in bubbles per second (inversely proportional).

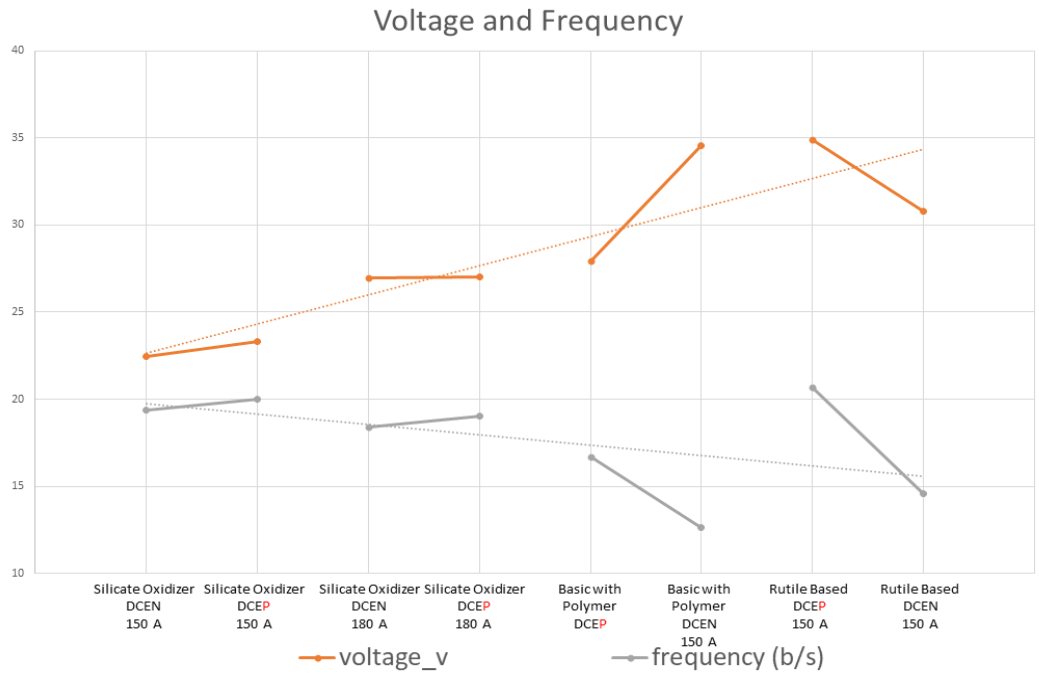

Figure 12 - Relationship between the average voltage and the average and maximum diameter of the bubble (directly proportional).

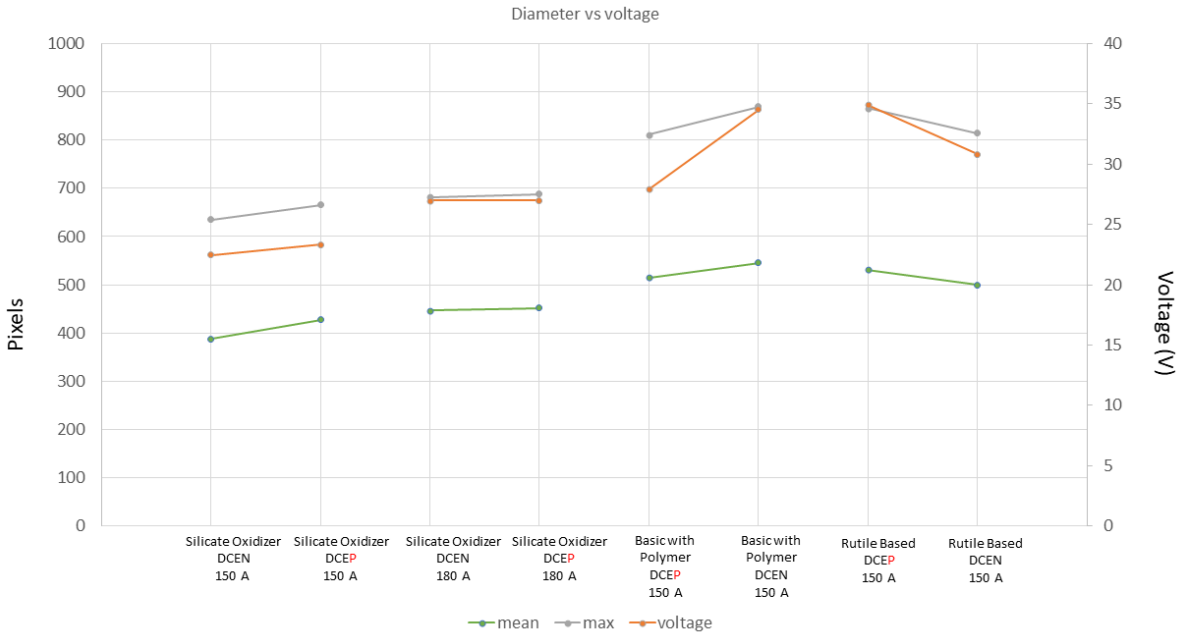

Figure 13- Relationship between the coefficient of variation of the process current and that of the diameter of the bubbles.

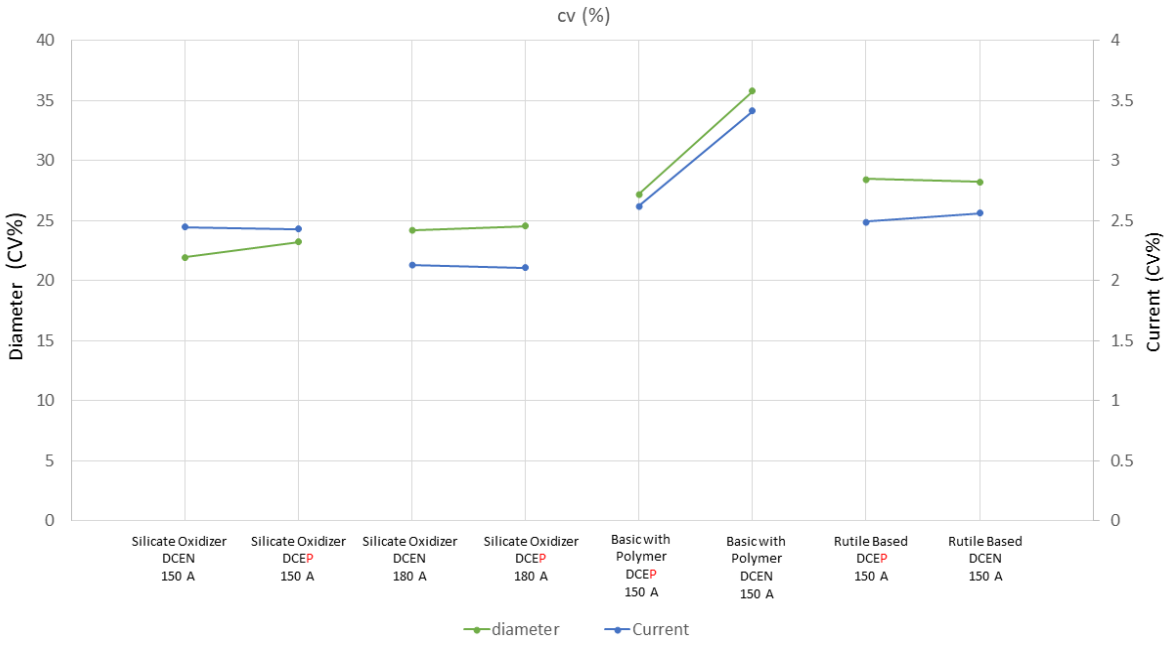

4.5 Generation of a bubble adjacent to the melting pool.

It was identified that the bubble is not always protecting the electric arc and is sometimes generated in the tail of the welding pool (Fig. 14). This is related to a continuous variation of the electrical parameters of the process (current welding and voltage welding). The generation of a bubble in the tail of the welding puddle pool was mentioned earlier by (WANG et al., 2019a) in his research with FCAW, where it is mentioned that a protective bubble at this location and at the melting pool is beneficial to the weld bead by decreasing the cooling rate of the metal compared to being fully exposed to the aqueous environment. Although nowadays a considerable amount of UWW research is focused in FCAW, many phenomena described in the literature are similar between both welding processes.

4.6 Comparison of all consumables at 150 A.

Comparing the computed results (Table 2) of the experiments of the three electrodes in a welding current of 150 A, it was identified that for the same welding conditions the relationship between the voltage values in the inverse and direct polarity were different and depending on the electrode. The average welding voltage in the inverse polarity for the silicate oxidizer and Rutile based electrodes were higher than the direct polarity. In the other hand, for the electrode

that contains polymer (basic) the result was the opposite. It was also appreciated that the commercial electrode with Rutile is the one with the highest average voltage for reverse polarity compared to the other electrodes, and, for a direct polarity the highest voltage was obtained with the basic with polymer electrode (The reasons will be discussed later when this electrode is explicitly mentioned). In addition, it was found that the Rutile-based (commercial) electrode had a lower coefficient of voltage variation (Table 2, cv (%) - voltage (video)) and a lower number of short circuits than in the other experiments (Fig. 15).

Figure 14 - Bubble generation the tail of the welding puddle.

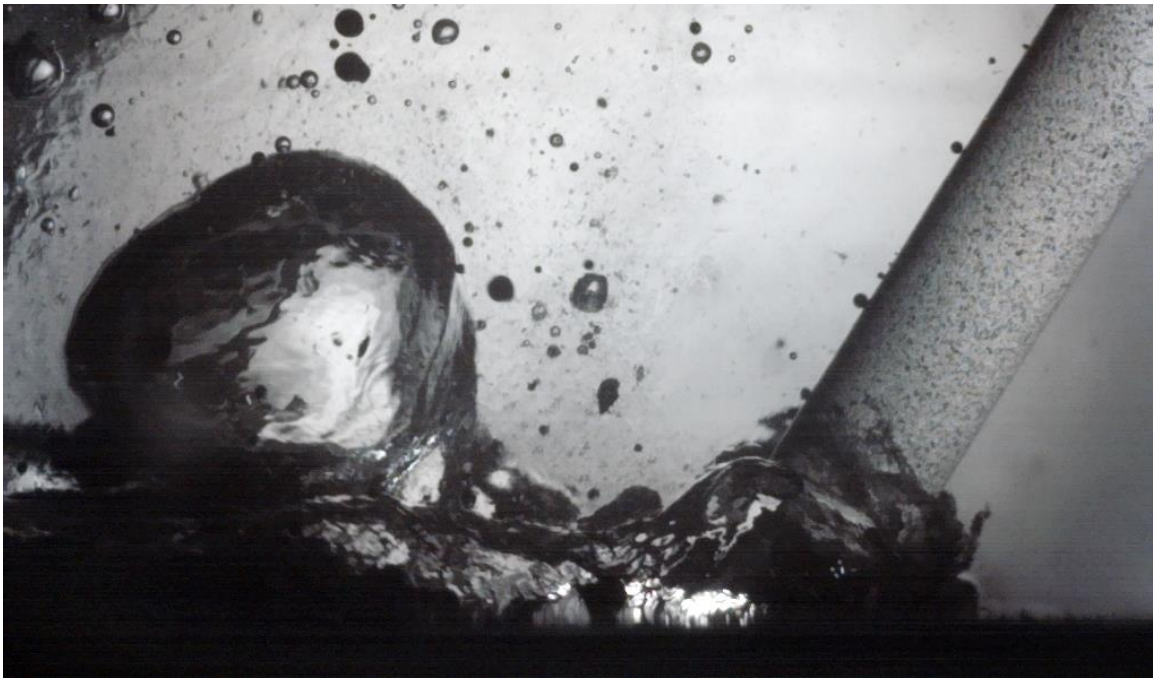

Figure 15 - The number of short circuits on each experiment.

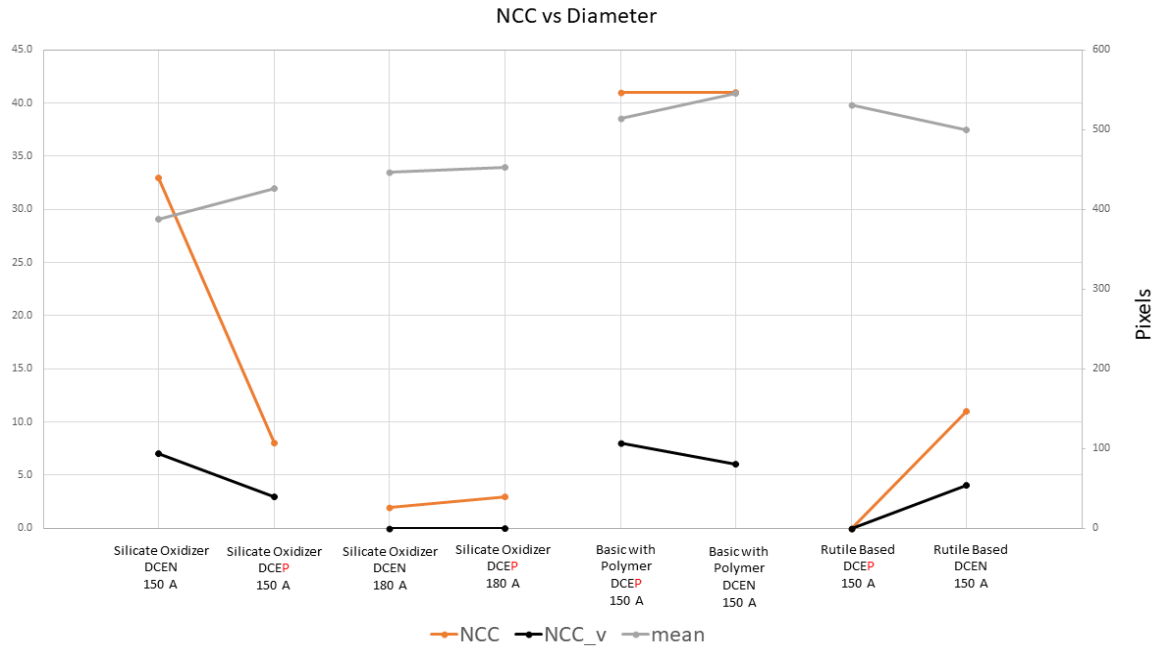

4.7 150 A vs 180A on silicate oxidizer electrode.

Making a comparison of the increased of the welding current from 150A to 180A for the silicate oxidizer electrode, it was identified that when increasing the welding current, the bubbles presented a larger diameter (Fig. 12) and their frequency (b/s) decreased for both polarities (Fig. 11). This, as already analyzed, it generates greater arc stiffness and it is related to greater stability (BERNARDI; GONÇALVES SILVA; SCHWEDERSKY, 2018; GUO et al., 2015; WANG et al., 2019b; YANG et al., 2019). In the visual analysis of the process, it was identified that with a greater diameter of the bubble it was possible to protect the arc for longer and, with a lower frequency of separation from the bubble, the time of direct exposure of the arc to the aqueous environment was shorter; which leads to a decrease in the number of the short circuits. Also, it is important to note that there were no short circuits in any of the polarities with a current of 180 A.

With regard to variations in welding current, in the calculation of the standard deviation of the voltage signals (Table 2, cv (%) - voltage (video)) for the silicate oxidizer electrode, with a

welding current of 150 A there is a greater dispersion of the voltage values than when the current is increased (180 A) for both polarities. This means that the current of the welding process is easier controlled by the welding source when 180 A.

4.8 Basic electrode with addition of PTFE.

With regard to the visual analysis of the electrode with the addition of PTFE in the direct polarity at 150 A, the observation suggests that, unlike the other experiments, during the formation of the bubble, the one adopts a *flakes-like* (video 4) appearance (Fig. 16) and it expands and contracts in volume oscillating before breaking into several smaller bubbles. The phenomenon of the bubble formation that this electrode presents when subjected to these welding parameters has not been previously discussed in the literature, however, ZHANG et al. (2019) relate the extinction of the welding arc with the subsequent collapse of the bubble in smaller objects. Even though, experiments with this electrode generated the highest number of short circuits compared to the other electrodes (Fig. 15), this bubble phenomenon was also observed in regions of relative stability (without the presence of short circuits nor voltage drops). With regard to this phenomenon, the literature mentions that the *arc bubble* is composed of a complex mixture of gases and that the formation of bubbles without significant collapses is essential for the stability of the electric arc, and consequently, essential for the improvement in the stability of the process (WANG et al., 2018c; YANG et al., 2020).

Figure 16 - Appearance of the electrode bubble (flakes) with addition of PTFE in direct polarity.

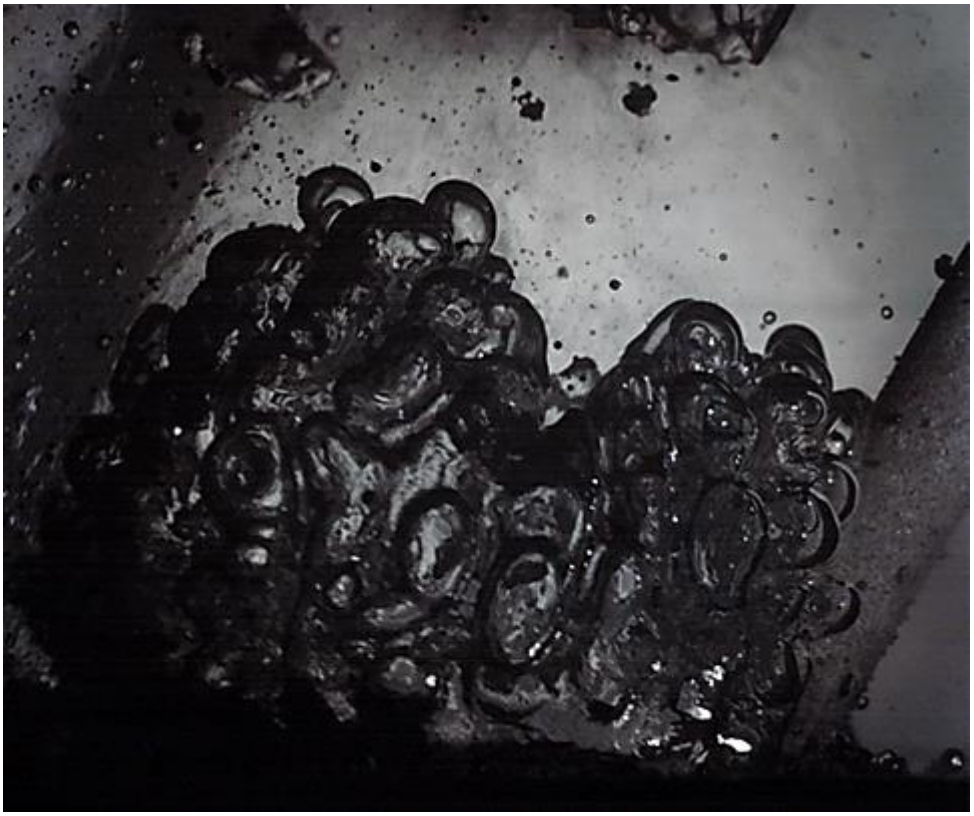

It was also observed that, for this experiment, the bubble diameter of this basic electrode was higher than that of the other two electrodes of the experiment (Fig. 13). Amaral et al. mention that PTFE particles provoke complex electrochemical and thermochemical reactions in the electric arc, resulting in the demand for a considerable amount of heat (AMARAL; MORENO-URIBE; BRACARENSE, 2021). In addition, Lancaster mentions that elements such as fluorine increase the electrical resistance of the plasma column and, in effect, this have a tendency to cause higher operating arc voltages for a given arc length, this is due to greater difficulties in the passageway of the electric current (RESENDE, 2013). According to Yang et al., with the increase in the arc voltage, the maximum diameter of the bubbles tends to increase (YANG et al., 2019). Therefore, taking into account the referenced literature, the increase in the diameter of the bubbles could be related to the presence of polymer particles in the addition material.

Another relevant aspect is, the coefficient of variation of the current for this electrode (with polymer) is greater than the other electrodes in both polarities (Fig. 13). The literature reports that this fact may be related to the fluoride content in the electrode, which tends to cause a more agitated, violent arc with higher rates of disturbances, causing greater instabilities of the arc (BANG; JUNG; HAN, 2010; MENEZES; PESSOA; BRACARENSE, 2019).

4.9 Arc Stability Analysis.

According to Amaral (2021), the study of the electric arc through electrical signals (welding current and voltage values) is a method that identifies various phenomena that occur during welding (AMARAL; MORENO-URIBE; BRACARENSE, 2021).

Thus, as mentioned above, a data acquisition system was used in order to obtain voltage and current values and then characterize the welding processes for each of the proposed conditions. In each analysis, data was used after 10 seconds of the process and at the moment that the process occurred within the visible field of the camera.

In Table 2 it was identified that the reverse polarity (DCEP) presents higher average voltage values for all experiments except for the basic electrode + polymer.

The results show that the commercial rutile-based electrode is the one with the highest average voltage for reverse polarity compared to the other electrodes and for direct polarity the highest voltage was obtained with the basic electrode. The rutile-based electrode also presented a lower voltage coefficient of variation and number of short circuits than the other experiments with 150A.

This stability trend presented in the calculation of the voltage variation coefficient can be reinforced with the forms of the histograms (figure 18). In the same way and the number of short circuits can be seen in the oscillograms of voltage and current in each of the experiments (figure 19 - 22).

Due to the magnitude of the signals over time, it can be seen that the metallic transfer, in most of the experiments, was not only due to a short circuit but also due to an electric arc, especially in the direct polarity.

For the welding carried out with the electrodes, in the histograms it can be observed that there is a greater concentration of points in a smaller area for the reverse polarity than the direct one in the experiments with the silicate oxidizer and rutile-based electrodes and what is presented is opposite for the basic electrode, confirming the result found in the calculation of the coefficient of variation of the current; with the exception of the rutile-based electrode, where the histogram shows a graph with less width and greater height for the forward polarity instead of the reverse, which would lead to a more stable process for the former.

In the case of the silicate oxidizer electrode, the histogram illustrates an increase in the stability of the process when the value of the current is increased to 180A. This trend holds for both polarities.

Another method proposed for measuring the stability through the study of the images is the time that the bubble is remining in the welding area (Fig. 17). The thesis is, the more time the bubble keeps on the welding area, the more time it will be protecting the weld. This permits to resume the information presented in a histogram to only one variable that is easier to analyze. However, it can be seen that, saying that this is an approximation variable that is related to stability, still could be influenced by interaction with other variables. An example of this, is shown in Fig. 17, where the basic electrode present high remaining values while having also a high of number of short circuits.

Figure 17 The time that the bubble is remining in the welding area (blue) and the diameter of the bubble (green).

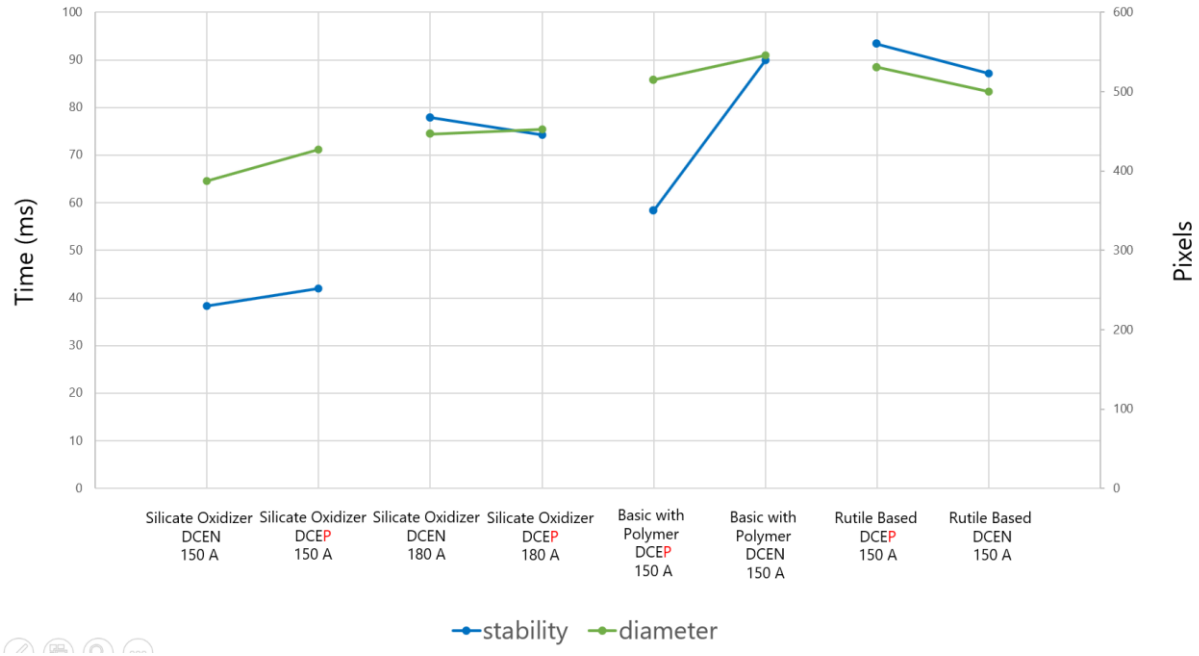

Figure 18 - Histograms (Voltage x Current) of the different experiments. On the left the DCEN experiments and on the right the DCEP (same order as in figure 8).

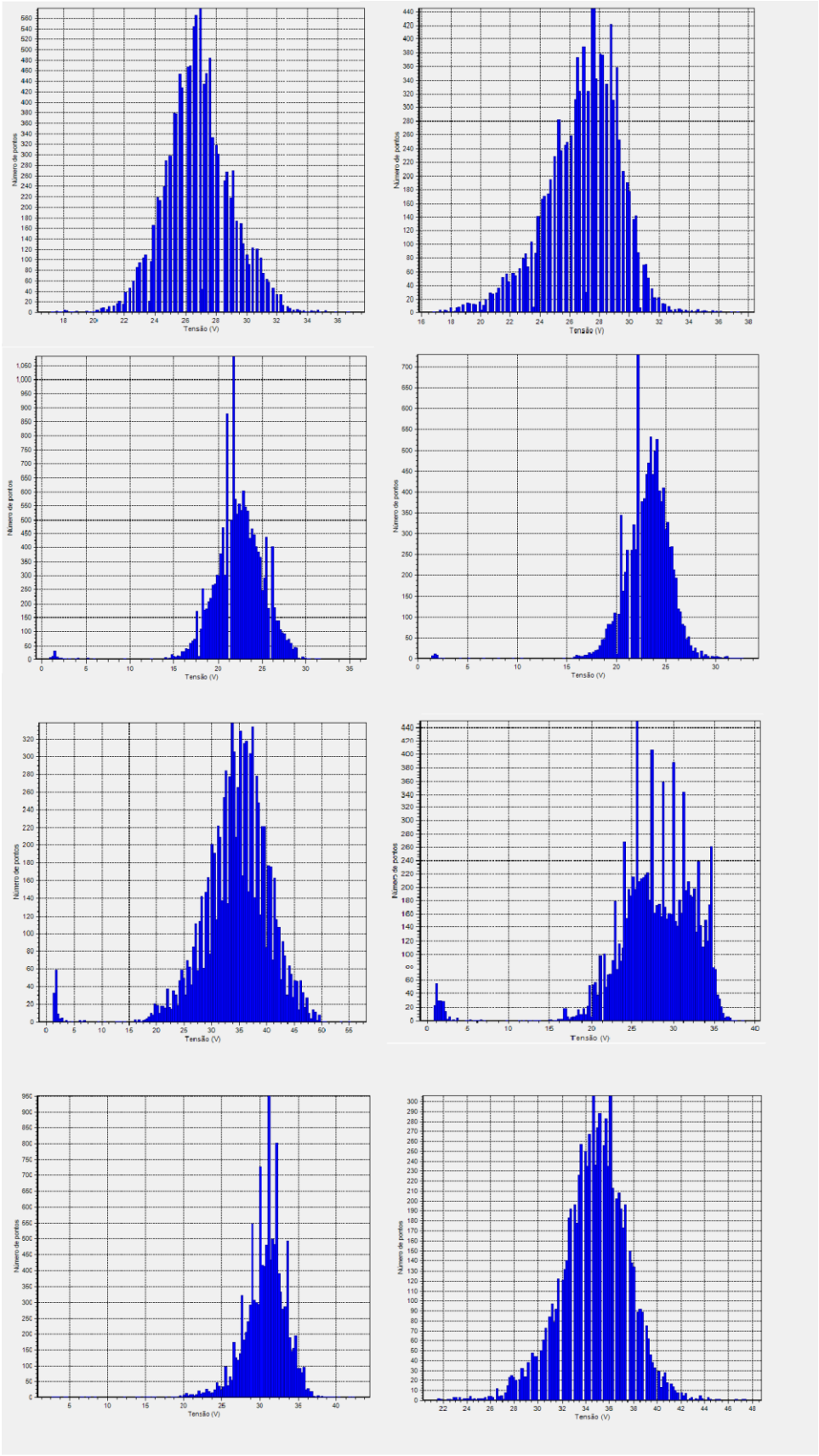

Figure 19 - Oscillograms Voltage (left) and Current (right) of WW70 180A. In the upper part the data taken in DCEN polarity and in the lower part the data obtained in DCEP polarity.

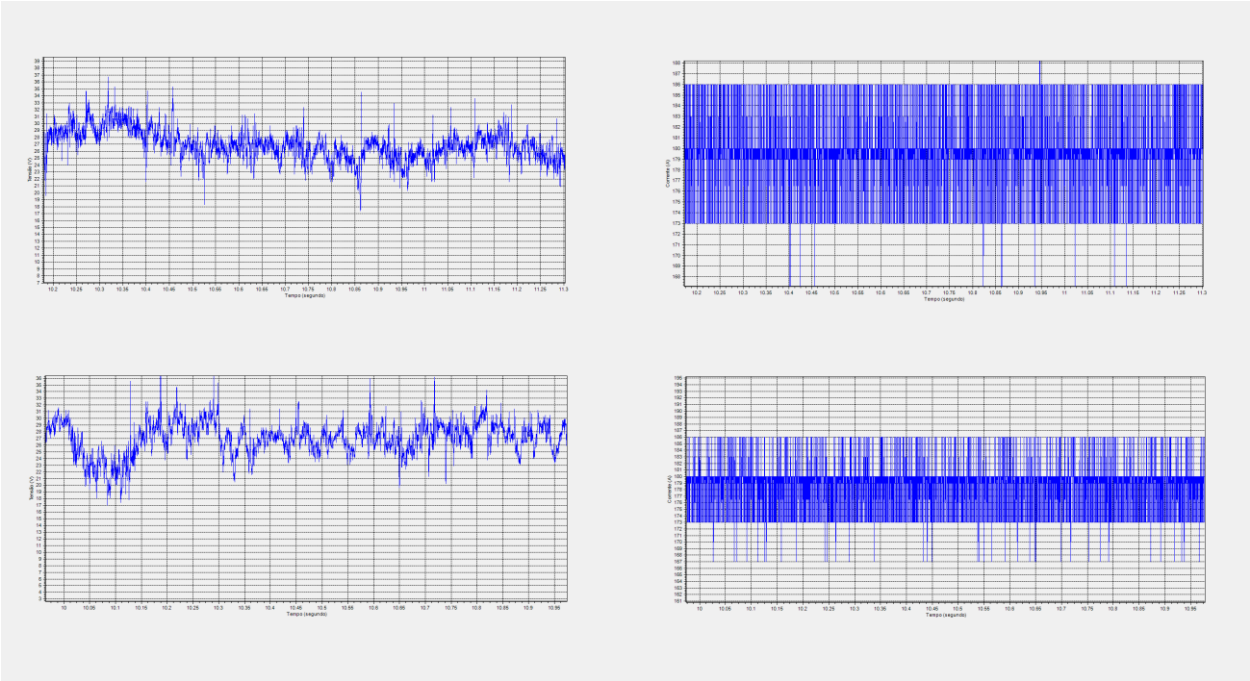

Figure 20 - Oscillograms Voltage (left) and Current (right) of WW70 150A. In the upper part, the data taken in DCEN polarity and in the lower part, the data obtained in DCEN polarity.

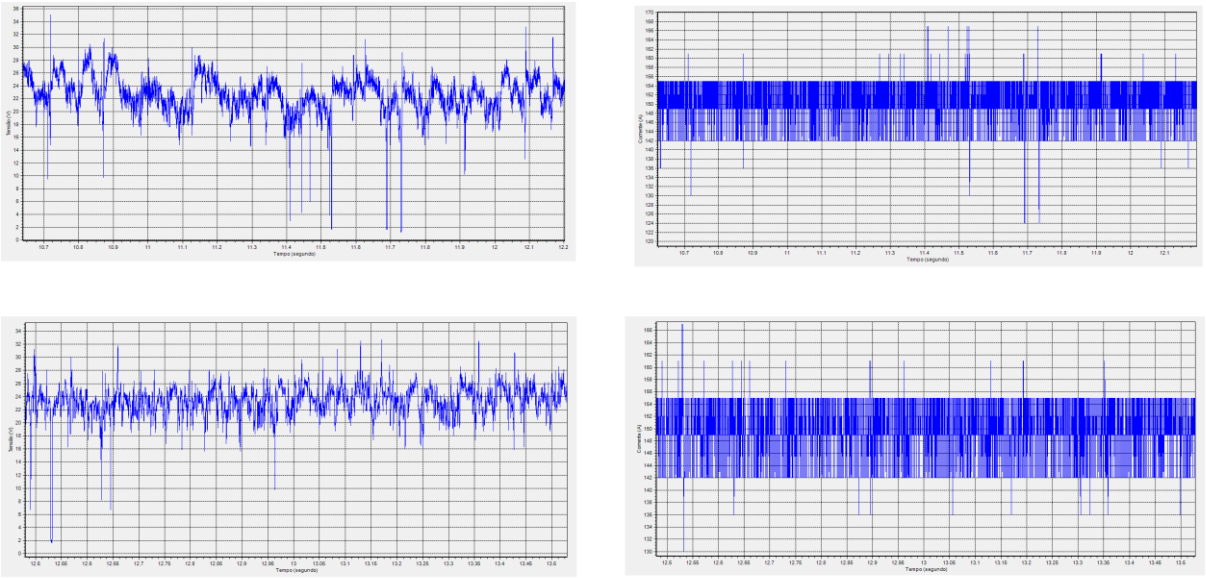

Figure 21 - Oscillograms Voltage (left) and Current (right) of Basic + PTFE 150A. In the upper part the data taken in DCEN polarity and in the lower part the data obtained in DCEP polarity.

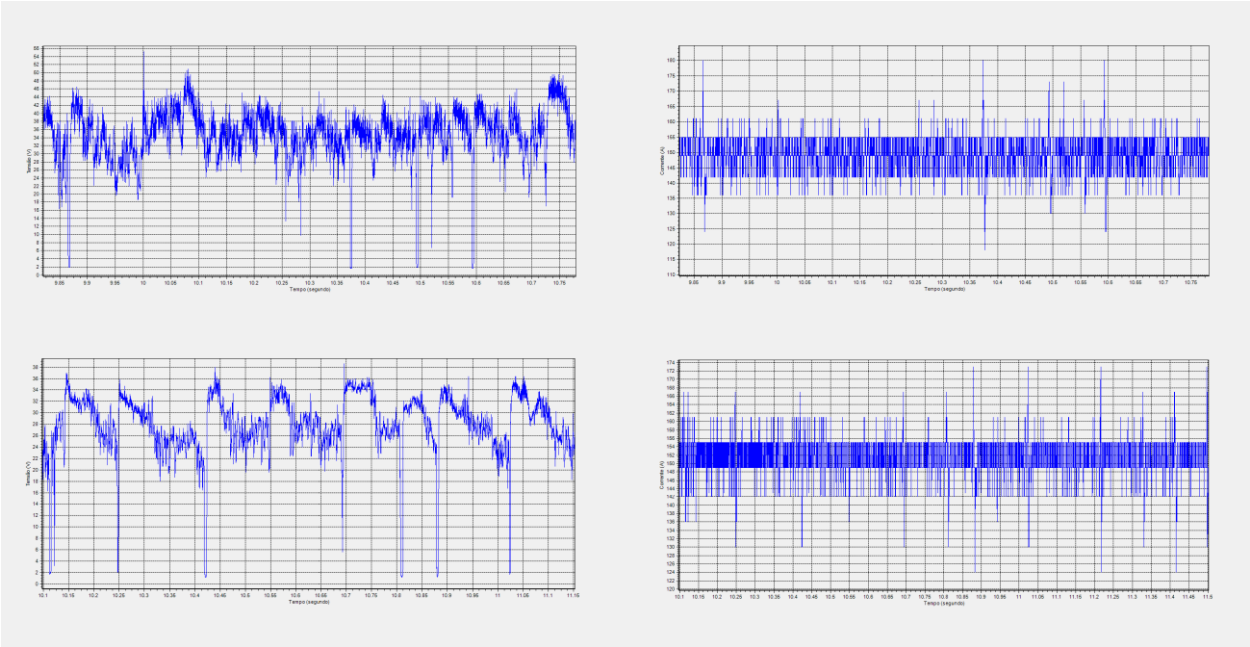

Figure 22 - Oscillograms Voltage (left) and Current (right) of Hydroweld FS 150A. In the upper part the data taken in DCEN polarity and in the lower part the data obtained in DCEP polarity.

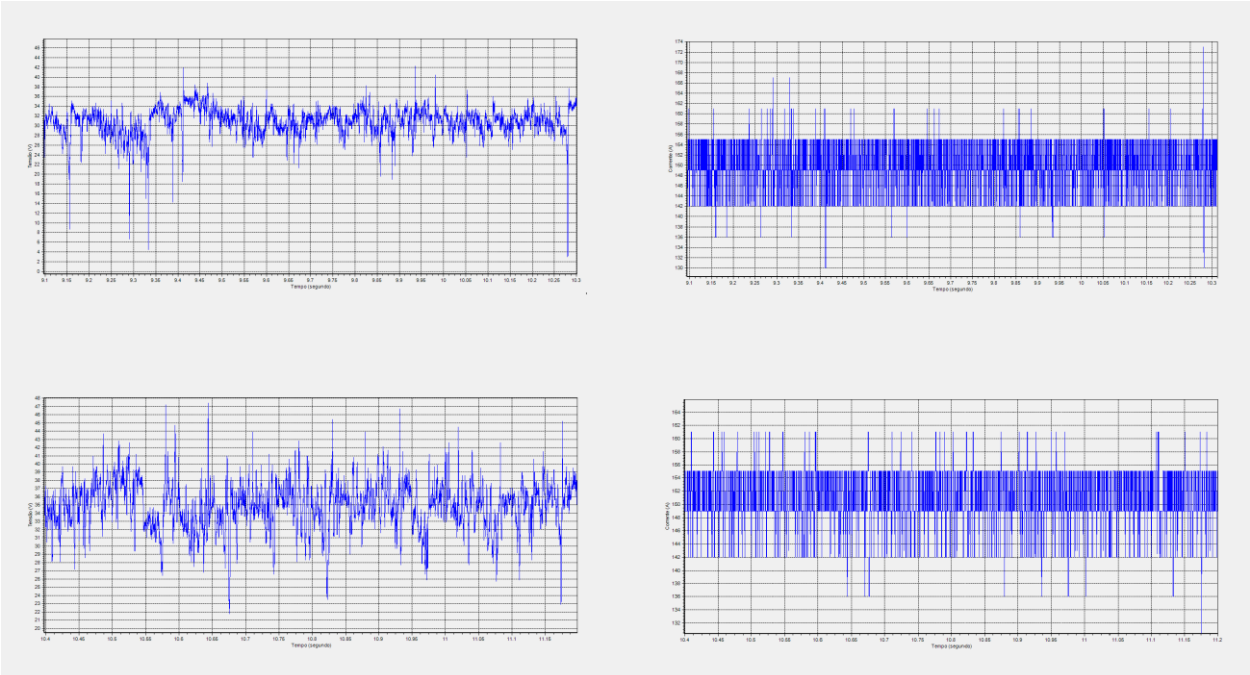

5. CONCLUSIONS

It was identified that the welding voltage presents a behavior similar to a sine wave and depending on the slope of the curve, its signal will have two specific directions, being able to be a positive slope during the growth of the bubble or a negative slope during its separation from the welding arc area.

In the experiments carried out it was found that in the moments in which the voltage decreases to values lower to 5 Volts, it does not explicitly mean that there is a short circuit, it is simply an attenuation of the arc.

It was observed that in the experiment with the silicate oxidizer electrode, at 150 A in DCEP, the voltage values in the valleys are higher than in the direct polarity and these are lower than 16V. So, it could be assumed that the transfer of material is not by short-circuit, but the behavior of the arc (oscillating in a sinusoidal form) reflects the dynamics of the bubbles.

A possible inversely proportional relationship between the mean voltage of the experiment and the frequency (in bubbles per second (b/s)) was also identified. And, a proportional relationship between this voltage and the calculated equivalent diameter. Also, there is a possible relationship between the coefficient of variation of the current and that of the diameter of the bubbles, however, this could only be valid for the consumables and welding parameters presented in this study.

For the silicate oxidizer electrode there were no short circuits in any of the polarities with a current of 180 A (DCEP & DCEN).

The observation of the experiment videos suggests that, unlike the other experiments, during the formation of the bubble, the basic electrode, agglomerated with a polymer, adopts a *flakes-like* appearance and it expands and contracts in volume oscillating before breaking into several smaller bubbles. Even though, experiments with this electrode generated the highest number of short circuits compared to the other electrodes, this bubble phenomenon was also observed in regions of relative stability (without the presence of short circuits nor voltage drops). Also, the increase in the diameter of the bubbles of this electrode could be related to the presence of polymer particles in the addition material.

With regard to the phenomenon of the bubble formation in the Rutile flux coated electrode, a smoother phenomenon of formation and detachment of the bubble was perceived, which it could be related to its greater stability in the electrical parameters of the process. This smoothness could also be observed in the histograms of the experiment belonging this electrode.

The study by calculating the projected area and the centroid of this area facilitated the results generated by the algorithm, allowing the detection and monitoring of the bubbles, as well as a possible improvement in the understanding of the interaction between them in order to improve the quality of the welding seam.

REFERENCES

A. Q. BRACARENSER. LACERDA DE SOUZAM. C. M. DE SOUZA COSTAP. E. FARIAS. LIU. **Welding current effect on diffusible hydrogen content in flux cored arc weld metal**. Journal of the Brazilian Society of Mechanical Sciences, *[S. l.]*, 2002. DOI: https://doi.org/10.1590/S0100-73862002000400005.

AMARAL, Erriston Campos; MORENO-URIBE, Andrés M.; BRACARENSE, Alexandre Queiroz. **Effects of PTFE on operational characteristics and diffusible H and O contents of weld metal in underwater wet welding**. Journal of Manufacturing Processes, *[S. l.]*, v. 61, p. 270–279, 2021. DOI: 10.1016/j.jmapro.2020.11.018.

ANDRADE, Luciano G. D.; DIAS, Weslley C.; RIBEIRO, Leandro F.; BRACARENSE, Alexandre Q.; PESSOA, Ezequiel C. P.; LIU, Stephen. **The effect of base metal and core rod carbon content on underwater wet welds porosity**. Soldagem e Inspecao, *[S. l.]*, v. 15, n. 2, p. 156–164, 2010. DOI: 10.1590/s0104-92242010000200010.

ARIAS, A. R.; BRACARENSE, A. Q. **Fatigue crack growth assessment in underwater wet welds**. Welding Journal, *[S. l.]*, v. 96, n. 8, p. 287S-294S, 2017.

BANG, Kook Soo; JUNG, Hong Chul; HAN, Il Wook. **Comparison of the effects of fluorides in rutile-type flux cored wire**. Metals and Materials International, *[S. l.]*, v. 16, n. 3, p. 489–494, 2010. DOI: 10.1007/s12540-010-0622-6.

BERNARDI, Rafael Albino; GONÇALVES SILVA, Régis Henrique; SCHWEDERSKY, Mateus Barancelli. **INVESTIGAÇÕES DE ORDEM OPERACIONAL E IMPLEMEN-TAÇÃO DE TECNOLOGIAS PARA SOLDAGEM SUBAQUÁ-TICA MOLHADA COM ELETRODOS REVESTIDOS**. 2018. *[S. l.]*, 2018.

BRACARENSE, A.; LIU, S. **Chemical composition variations in shielded metal arc welds**. Welding journal, *[S. l.]*, v. 72, n. 12, p. 529, 1993.

BRACARENSE, Alexandre Q.; PESSOA, Ezequiel C.; DOS SANTOS, Valter R.; MONTEIRO, Maurício J.; RIZZO, Fernando C.; PACIORNIK, Sidnei; REPPOLD, Ricardo; DOMINGUES, José R.; VIEIRA, Leonardo A. **Estudo comparativo de eletrodos comerciais para soldagem subaquática molhada**. Soldagem e Inspecao, *[S. l.]*, v. 15, n. 4, p. 325–335, 2010. DOI: 10.1590/S0104-92242010000400010.

BRADISKI, G. **The OpenCV Library**. [s.l.] : Journal of Software Tools, 2000.

CHEN, Bo; FENG, Jicai. **Modeling of underwater wet welding process based on visual and arc sensor**. Industrial Robot, *[S. l.]*, v. 41, n. 3, p. 311–317, 2014. DOI: 10.1108/IR-03-2014-0315.

CHEN, Bo; JIA, Chuanbao; FENG, Jicai. **Underwater wet weld seam tracking based on passive visual sensor**. *In*: ADVANCED MATERIALS RESEARCH 2013a, **Anais** [...]. [s.l: s.n.] p. 725–728. DOI: 10.4028/www.scientific.net/AMR.683.725.

CHEN, Bo; JIA, Chuanbao; FENG, Jicai. **Active visual sensor based weld seam tracking for underwater wet welding**. *In*: ADVANCED MATERIALS RESEARCH 2013b, **Anais** [...]. [s.l: s.n.] p. 588–591. DOI: 10.4028/www.scientific.net/AMR.717.588.

CHEN, Hao; GUO, Ning; HUANG, Lu; ZHANG, Xin; FENG, Jicai; WANG, Guodong. **Effects of arc bubble behaviors and characteristics on droplet transfer in underwater wet welding using in-situ imaging method**. Materials and Design, *[S. l.]*, v. 170, 2019. DOI: 10.1016/j.matdes.2019.107696.

CHEN, Hao; GUO, Ning; LIU, Cheng; ZHANG, Xin; XU, Changsheng; WANG, Guodong. **Insight into hydrostatic pressure effects on diffusible hydrogen content in wet welding joints using in-situ X-ray imaging method**. International Journal of Hydrogen Energy, *[S. l.]*, v. 45, n. 16, p. 10219–10226, 2020. a. DOI: 10.1016/j.ijhydene.2020.01.195. Disponível em: https://doi.org/10.1016/j.ijhydene.2020.01.195.

CHEN, Hao; GUO, Ning; SHI, Xianghua; DU, Yongpeng; FENG, Jicai; WANG, Guodong. **Effect of water flow on the arc stability and metal transfer in underwater flux-cored wet welding**. Journal of Manufacturing Processes, *[S. l.]*, v. 31, p. 103–115, 2018. DOI: 10.1016/j.jmapro.2017.11.010.

CHEN, Hao; GUO, Ning; XU, Kexin; XU, Changsheng; ZHOU, Li; WANG, Guodong. **In-situ observations of melt degassing and hydrogen removal enhanced by ultrasonics in underwater wet welding**. Materials and Design, *[S. l.]*, v. 188, p. 108482, 2020. b. DOI: 10.1016/j.matdes.2020.108482. Disponível em: https://doi.org/10.1016/j.matdes.2020.108482.

DE ARAUJO, Douglas; VILARINHO, Louriel; ALVES DE RESENDE, André. **INVESTIGAÇÃO DA TRANSFERÊNCIA METÁLICA POR MEIO DO PROCESSAMENTO DIGITAL DE IMAGEM**. [s.l: s.n.]. Disponível em: https://www.researchgate.net/publication/303821044.

DE ROSA OLIVEIRA, F. **Estudo sobre o correlacionamento do fenômeno das bolhas, sinais elétricos e metal de solda na soldagem subaquática molhada com eletrodos revestidos**. 2012. *[S. l.]*, 2012.

DE ROSA OLIVEIRA, Frederico; SOARES, William Rodrigues; BRACARENSE, Alexandre Queiroz. **Study correlating the bubble phenomenon and electrical signals in underwater wet welding with covered electrodes**. Welding International, *[S. l.]*, v. 29, n. 5, p. 363–371, 2015. DOI: 10.1080/09507116.2014.932980.

ESMERIO MAZZAFERRO, José Antônio. **Estudo da Estabilidade do Arco Elétrico na Soldagem Subaquática com Eletrodos Revestidos**. 1998. *[S. l.]*, 1998.

FENG, Jicai; WANG, Jianfeng; SUN, Qingjie; ZHAO, Huanyao; WU, Laijun; XU, Pengwei. **Investigation on dynamic behaviors of bubble evolution in underwater wet flux-cored arc welding**. Journal of Manufacturing Processes, *[S. l.]*, v. 28, p. 156–167, 2017. DOI: 10.1016/j.jmapro.2017.06.003.

GIRÓN CRUZ, FABIÁN EDUARDO. **UMA METODOLOGIA PARA MONITORAMENTO EM TEMPO REAL DOS MODOS DE TRANSFERÊNCIA DE METAL CONVENCIONAIS NO PROCESSO DE SOLDAGEM GMAW.** 2019. *[S. l.]*, 2019.

GOMES MAIA, Tereza Cristina; FLORES, Edna Lúcia; SCOTTI, Américo. **QUANTIFICAÇÃO DA TRANSFERENCIA METÁLICA NO PROCESSO MIG / MAG POR PROCESSAMENTO DE IMAGENS**. *[S. l.]*, 2002.

GUO, Ning; DU, Yongpeng; FENG, Jicai; GUO, Wei; DENG, Zongquan. **Study of underwater wet welding stability using an X-ray transmission method**. Journal of Materials Processing Technology, *[S. l.]*, v. 225, p. 133–138, 2015. DOI: 10.1016/j.jmatprotec.2015.06.003.

JIA, C. B.; ZHANG, Y.; ZHAO, B.; HU, J. K.; WU, C. S. **Visual Sensing of the Physical Process During Underwater Wet FCAW**. Welding Journal, *[S. l.]*, v. 95, p. 202s-209s, 2016.

JIA, Chuanbao; ZHANG, Yong; WU, Junfei; XING, Changjian; ZHAO, Bo; CHUANSONG, Wu. **Comprehensive analysis of spatter loss in wet FCAW considering interactions of bubbles, droplets and arc – Part 2: Visualization & mechanisms**. Journal of Manufacturing Processes, *[S. l.]*, v. 40, p. 105–112, 2019. a. DOI:

10.1016/j.jmapro.2019.03.011.

JIA, Chuanbao; ZHANG, Yong; WU, Junfei; XING, Changjian; ZHAO, Bo; WU, Chuansong. **Comprehensive analysis of spatter loss in wet FCAW considering interactions of bubbles, droplets and arc – Part 1: Measurement and improvement**. Journal of Manufacturing Processes, *[S. l.]*, v. 40, p. 122–127, 2019. b. DOI: 10.1016/j.jmapro.2019.03.013.

KALAKUNTLA, Shashank; ANDRIAMANALIMANANA, Bruno R. **Detection of Brain Tumor in Magnetic Resonance Imaging (MRI) Images using Fuzzy C-Means and Thresholding Detection of Brain Tumor in Magnetic Resonance Imaging (MRI) Department of Computer Sciences Utica , New York In Partial fulfillment Of the Requir**. 2021. SUNY Polytechnic Institute, *[S. l.]*, 2021. Disponível em: https://soar.suny.edu/handle/20.500.12648/1610.

KLETT, Jan; HECHT-LINOWITZKI, Vitali; GRÜNZEL, Oliver; SCHMIDT, Emily; MAIER, Hans Jürgen; HASSEL, Thomas. **Effect of the water depth on the hydrogen content in SMAW wet welded joints**. SN Applied Sciences, *[S. l.]*, v. 2, n. 7, p. 1–14, 2020. DOI: 10.1007/s42452-020-3066-8. Disponível em: https://doi.org/10.1007/s42452-020-3066-8.

ŁABANOWSKI, Jerzy. **Development of under-water welding techniques**. Welding International, *[S. l.]*, v. 25, n. 12, p. 933–937, 2011. DOI: 10.1080/09507116.2010.540847.

LI, Hong Liang; LIU, Duo; YAN, Yao Tian; GUO, Ning; LIU, Yi Bo; FENG, Ji Cai. **Effects of heat input on arc stability and weld quality in underwater wet flux-cored arc welding of E40 steel**. Journal of Manufacturing Processes, *[S. l.]*, v. 31, p. 833–843, 2018. DOI: 10.1016/j.jmapro.2018.01.013.

LI, Zhigang; YANG, Liting; HUANG, Wei; YE, Jianxiong. **Feasibility analysis of image signal replaced by sound pressure in wet welding under depth water environment**. Hanjie Xuebao/Transactions of the China Welding Institution, *[S. l.]*, v. 41, n. 8, p. 29–33, 2020. DOI: 10.12073/j.hjxb.20200422001.

LIU, Sang; JIGUANG, Zhong; YONGHUA, Shi; WANG, Guorong. **Image acquisition and processing of arc area in wet underwater welding**. Mechanics and Electronics, *[S. l.]*, v. 03, n. Qi, p. 15–17, 2000.

LIU, Stephen; PESSOA, E. C.; RIBEIRO, L. F.; BRACARENSE, A. Q.; DIAS, W. C.;

ANDRADE, L. G.; MONTEIRO, M. C. J. **ARC STABILITY INDEXES EVALUATION ON UNDERWATER WET WELDING**. *In*: PROCEEDINGS OF THE ASME 2010 29TH INTERNATIONAL CONFERENCE ON OCEAN, OFFSHORE AND ARCTIC ENGINEERING 2010, **Anais** [...]. : OMAE2010, 2010. p. 1–7.

MASUBUCHI, K.; TSAI, C. L. **Interpretive report on underwater welding**. Welding Research Council Bulletin, *[S. l.]*, v. 224, p. 37, 1977.

MATLAB. Natick, MassachusettsThe MathWorks Inc., , 2010.

MENDONÇA, Camilla Mara; BRACARENSE, Alexandre Queiroz. **Investigation of Bubbles Phenomenon in Underwater Wet Welding with Self-Protected Tubular Wire**. Soldagem e Inspecao, *[S. l.]*, v. 24, 2019. DOI: 10.1590/0104-9224/SI24.16.

MENEZES, Pedro Henrique Ribeiro; PESSOA, Ezequiel Caires Pereira; BRACARENSE, Alexandre Queiroz. **Comparison of underwater wet welding performed with silicate and polymer agglomerated electrodes**. Journal of Materials Processing Technology, *[S. l.]*, v. 266, n. April 2018, p. 63–72, 2019. DOI: 10.1016/j.jmatprotec.2018.10.019. Disponível em: https://doi.org/10.1016/j.jmatprotec.2018.10.019.

MORENO-URIBE, Andrés M. **EFEITO DA POLARIDADE SOBRE A MORFOLOGIA E ESTABILIDADE DE SOLDAS SUBAQUÁTICAS MOLHADAS COM ELETRODOS E6013 E WW70**. [s.l: s.n.].

ORTIZ, J. L.; MORENO-URIBE, A. M.; ACEVEDO, B. R.; LIMA, E. J.; ARIAS, A. R. **Application of computer vision techniques for contour detection in underwater wet welding: an exploratory study**. Journal of Physics: Conference Series, *[S. l.]*, v. 2046, n. 1, 2021. DOI: 10.1088/1742-6596/2046/1/012072.

PESSOA, Ezequiel Caires Pereira; BRACARENSE, Alexandre Queiroz; ZICA, Eduardo Maluf; LIU, Stephen; PEREZ-GUERRERO, Faustino. **Porosity variation along multipass underwater wet welds and its influence on mechanical properties**. Journal of Materials Processing Technology, *[S. l.]*, v. 179, n. 1–3, p. 239–243, 2006. DOI: 10.1016/j.jmatprotec.2006.03.071.

QUINN, T. P.; BRACARENSE, A. Q.; LIU, S. **A melting rate and temperature distribution model for shielded metal arc welding electrodes**. Welding Journal (Miami, Fla), *[S. l.]*, v. 76, n. 12, p. 532- s, 1997.

RESENDE, André Alves De. **Estudo de características operacionais do processo "Plasma-MIG" com arcos concêntricos - CAPÍTULO V**. 2013. *[S. l.]*, 2013.

RIBES VIVÓ, Carlos. **Estudio de ondas ultrasónicas para estabilizar el arco en soldadura con arco metálico sumergido bajo agua**. *[S. l.]*, 2020. Disponível em: https://riunet.upv.es:443/handle/10251/140619. Acesso em: 7 set. 2022.

ROSAS, Cristhian Harley Madariaga; MODENESI, Paulo José; ORTIZ, Mauricio Rincón. **Efectos de los Active Flux sobre Soldaduras GMAW Aplicadas a un Acero AISI/SAE 1020**. Soldagem & Inspeção, *[S. l.]*, v. 25, p. 1–12, 2020. DOI: 10.1590/0104-9224/si25.02.

ROWE, M.; LIU, S. **Recent developments in underwater wet welding**. Science and Technology of Welding and Joining, *[S. l.]*, v. 6, n. 6, p. 387–396, 2001. DOI: 10.1179/stw.2001.6.6.387.

SANTANA, Ivan José De; MODENESI, Paulo J. **Mathematical Modeling of GMA Welding - Free Fligth Transfer**. Soldagem & Inspeção, *[S. l.]*, v. 16, n. 3, p. 213–222, 2011. Disponível em: https://www.scielo.br/j/si/a/ffxvybQ9JNHG8TFvcTWrvCz/?format=pdf&lang=pt.

SOLDAGEM BMI. **SAP – V 4 + V4Ti + V4CTi Manual do sistema**. [s.l: s.n.]. Disponível em: https://www.imc-soldagem.com.br/media/com_eshop/attachments/manual_SAP V4_4aEd.pdf.

STURDEVANT, M.; HOLLINGER, M. ..; CHITIVELI, S. **Object tracking in video with OpenCV and Deep Learning**. 2020. Disponível em: https://developer.ibm.com/technologies/artificial-intelligence/patterns/detect-track-and-count-cars-in-a-video/.

URIBE, Andrés Mauricio Moreno; BRACARENSE, Alexandre Queiroz; PESSOA, Ezequiel Caires Pereira; DOS SANTOS, Valter Rocha. **Influência da polaridade sobre a estabilidade do processo de soldagem subaquática molhada com eletrodo revestido**. Soldagem e Inspecao, *[S. l.]*, v. 22, n. 4, p. 429–441, 2017. DOI: 10.1590/0104-9224/SI2204.13.

VAZ, Cláudio Turani; BRACARENSE, Alexandre Queiroz. **The Effect of the Use of PTFE as a Covered-Electrode Binder on Metal Transfer**. Soldagem & Inspeção, *[S. l.]*, v. 20, n. 2, p. 160–170, 2015. DOI: 10.1590/0104-9224/si2002.04.

WANG, Jianfeng; SUN, Qingjie; JIANG, Yunlu; ZHANG, Tao; MA, Jiangkun; FENG, Jicai. **Analysis and improvement of underwater wet welding process stability with static mechanical constraint support**. Journal of Manufacturing Processes, *[S. l.]*, v. 34, p. 238–250, 2018. a. DOI: 10.1016/j.jmapro.2018.06.007.

WANG, Jianfeng; SUN, Qingjie; PAN, Zuchen; YANG, Jie; FENG, Jicai. **Effects of welding speed on bubble dynamics and process stability in mechanical constraint-assisted underwater wet welding of steel sheets**. Journal of Materials Processing Technology, *[S. l.]*, v. 264, p. 389–401, 2019. a. DOI: 10.1016/j.jmatprotec.2018.09.022.

WANG, Jianfeng; SUN, Qingjie; ZHANG, Shun; LIU, Yibo; FENG, Jicai. **Investigation on Underwater Wet Welding Process Stability Based on the Arc Bubble Control**. Jixie Gongcheng Xuebao/Journal of Mechanical Engineering, *[S. l.]*, v. 54, n. 14, p. 50–57, 2018. b. DOI: 10.3901/JME.2018.14.050.

WANG, Jianfeng; SUN, Qingjie; ZHANG, Shun; WANG, Chengjin; WU, Laijun; FENG, Jicai. **Characterization of the underwater welding arc bubble through a visual sensing method**. Journal of Materials Processing Technology, *[S. l.]*, v. 251, p. 95–108, 2018. c. DOI: 10.1016/j.jmatprotec.2017.08.019.

WANG, Jianfeng; SUN, Qingjie; ZHANG, Tao; XU, Pengwei; FENG, Jicai. **Experimental study of arc bubble growth and detachment from underwater wet FCAW**. Welding in the World, *[S. l.]*, v. 63, n. 6, p. 1747–1759, 2019. b. DOI: 10.1007/s40194-019-00776-3.

WANG, Leilei; XIE, Fangxiang; FENG, Yunliang; WANG, Zhenmin. **Innovative methodology and database for underwater robot repair welding: A technical note**. ISIJ International, *[S. l.]*, v. 57, n. 1, p. 203–205, 2017. DOI: 10.2355/isijinternational.ISIJINT-2016-407.

WU, JUNFEI; HAN, YANFEI; JIA, CHUANBAO; YANG, QINGYUAN; WU, CHUANSONG. **Underwater Pulse-Current FCAW - Part 2: Bubble Behaviors and Waveform Optimization**. Welding Journal, *[S. l.]*, v. 99, n. 12, p. 303s-311s, 2020. DOI: 10.29391/2020.99.028. Disponível em: https://s3.amazonaws.com/WJ-www.aws.org/supplement/2020.99.028.pdf.

YANG, Qingyuan; HAN, Yanfei; JIA, Chuanbao; DONG, Shengfa; WU, Chuansong. **Visual Investigation on the Arc Burning Behaviors and Features in Underwater Wet FCAW**. Journal of Offshore Mechanics and Arctic Engineering, *[S. l.]*, v. 142, n. 4, 2020. DOI:

10.1115/1.4045914.

YANG, Qingyuan; HAN, Yanfei; JIA, Chuanbao; WU, Junfei; DONG, Shengfa; WU, Chuansong. **Impeding effect of bubbles on metal transfer in underwater wet FCAW**. Journal of Manufacturing Processes, *[S. l.]*, v. 45, p. 682–689, 2019. DOI: 10.1016/j.jmapro.2019.08.013.

ZHANG, Yong; JIA, Chuanbao; WANG, Jianxin; ZHAO, Bo; WU, Chuansong. **Investigation on the bubble dynamic behaviors and corresponding regulation method in underwater flux-cored arc welding**. Proceedings of the Institution of Mechanical Engineers, Part B: Journal of Engineering Manufacture, *[S. l.]*, v. 233, n. 7, p. 1808–1817, 2019. DOI: 10.1177/0954405418789983.

6. Appendix A

In this section, the characteristics of the electrodes, plot before together, are illustrated individually. This, for a better understanding of the impact of each factor on the sensed parameters.

1. Silicate Oxidizer electrode.

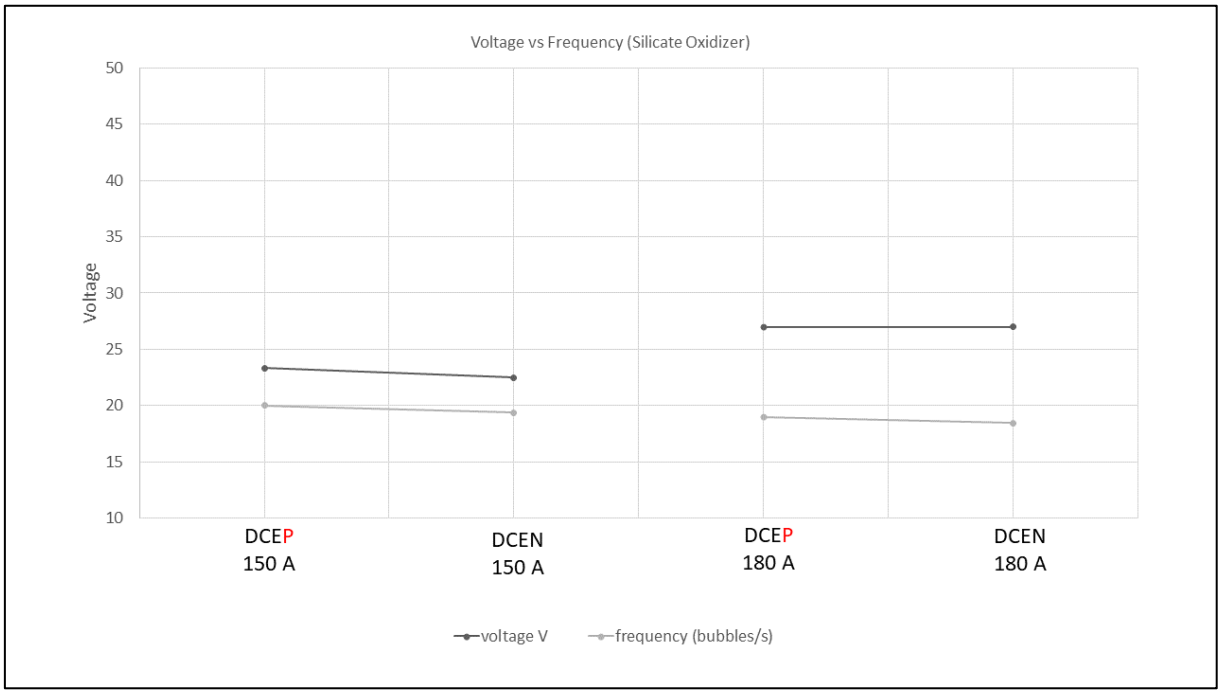

Figure A.1.1 Voltage vs Frequency.

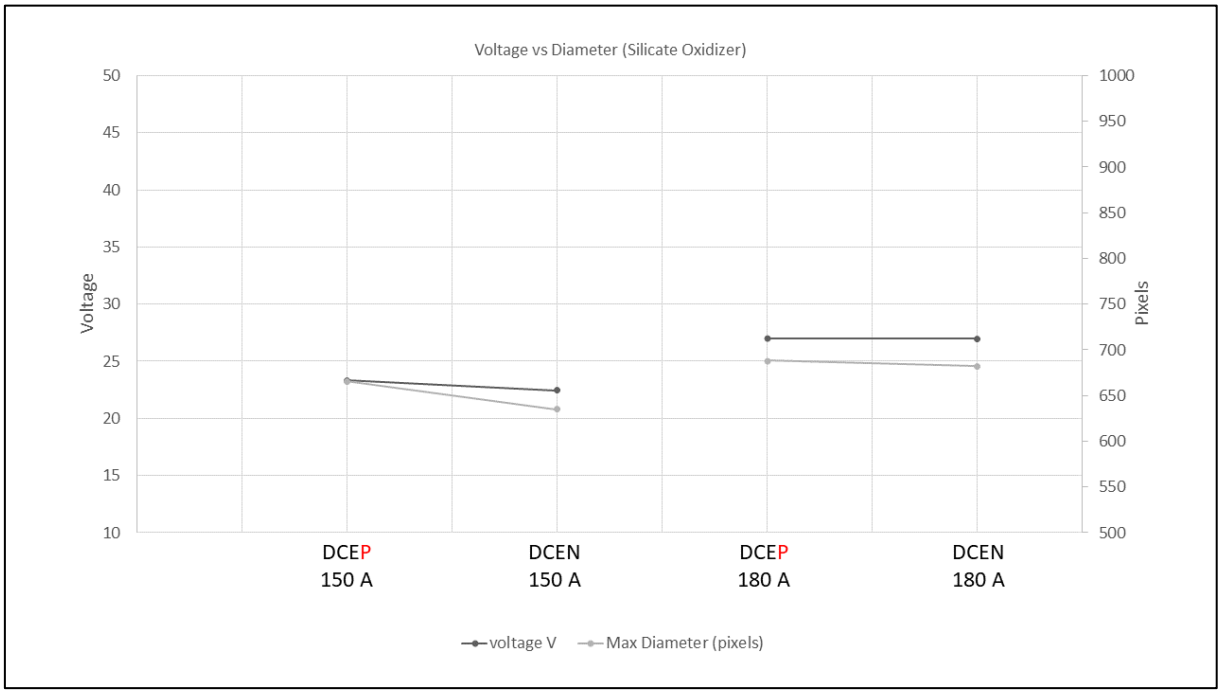

Figure A.1.2 Voltage vs Diameter.

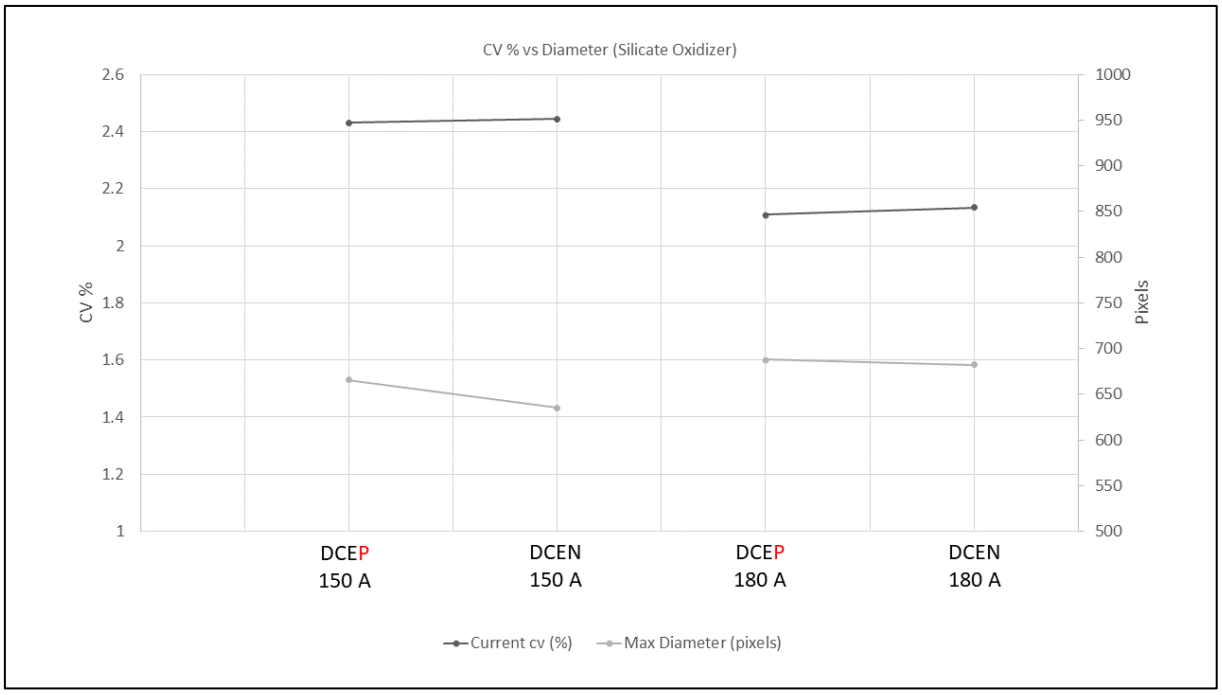

Figure A.1.3 Coefficient of variation of the current **(**CV%) vs Diameter.

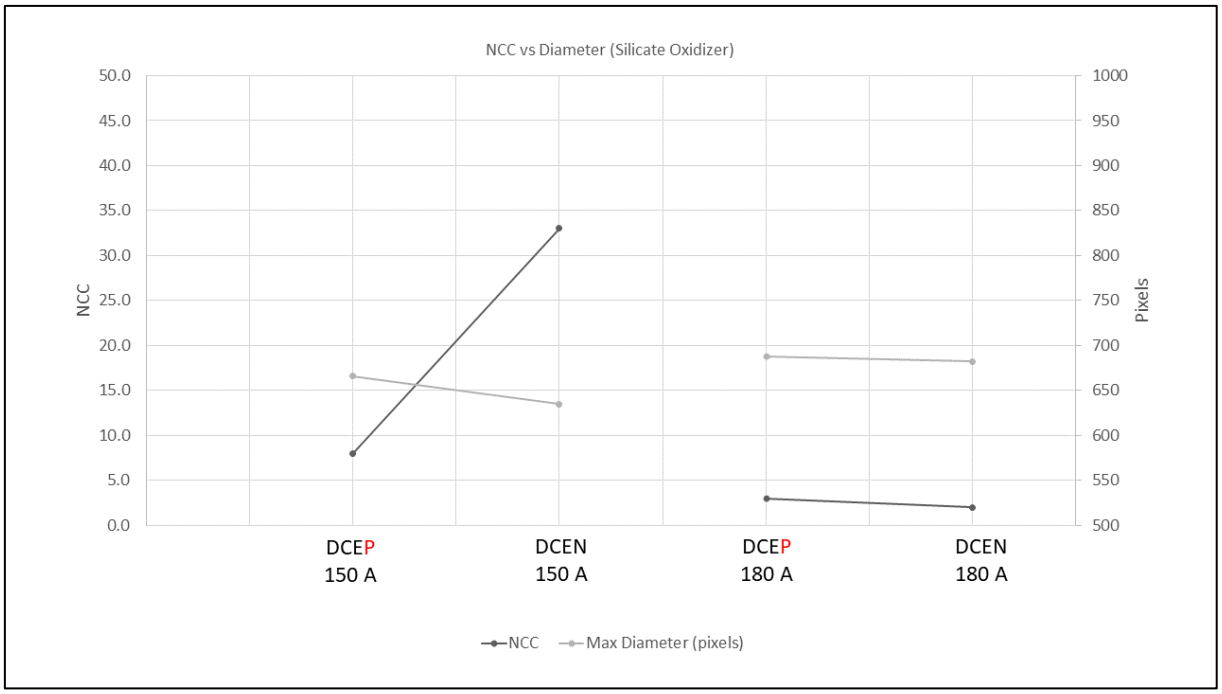

Figure A.1.4 Number of short circuits (NCC) vs Diameter.

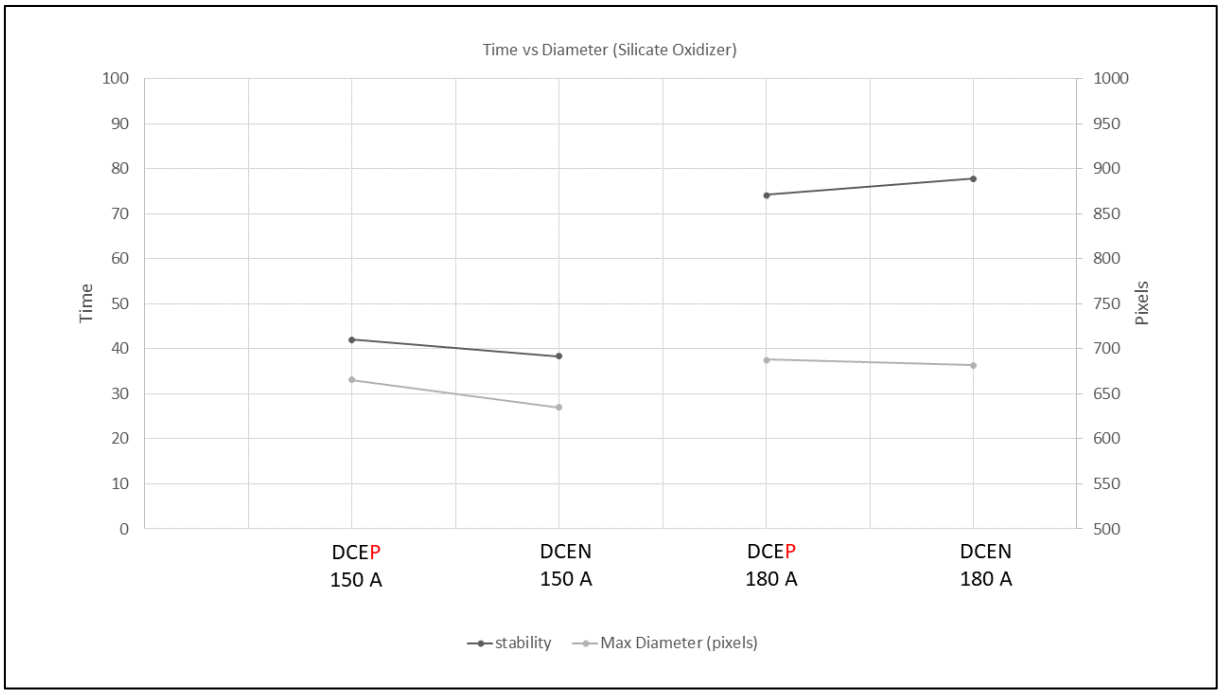

Figure A.1.5 Time remaining in the welding zone vs Diameter.

2. Basic with polymer electrode.

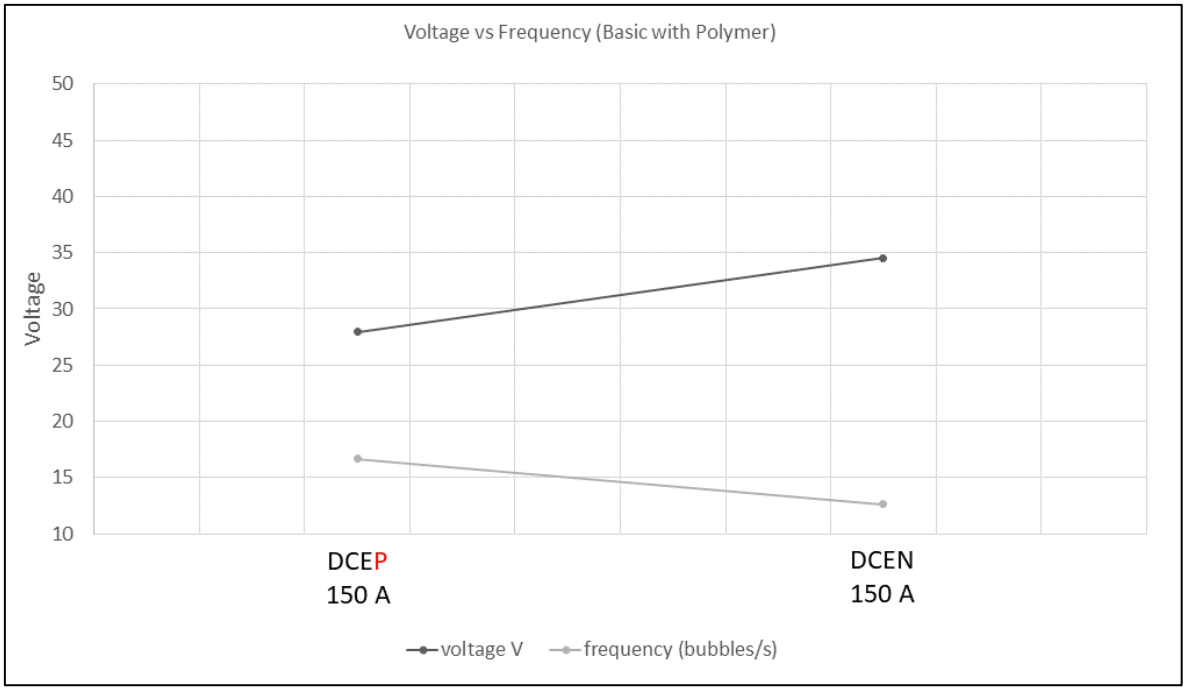

Figure A.2.1 Voltage vs Frequency.

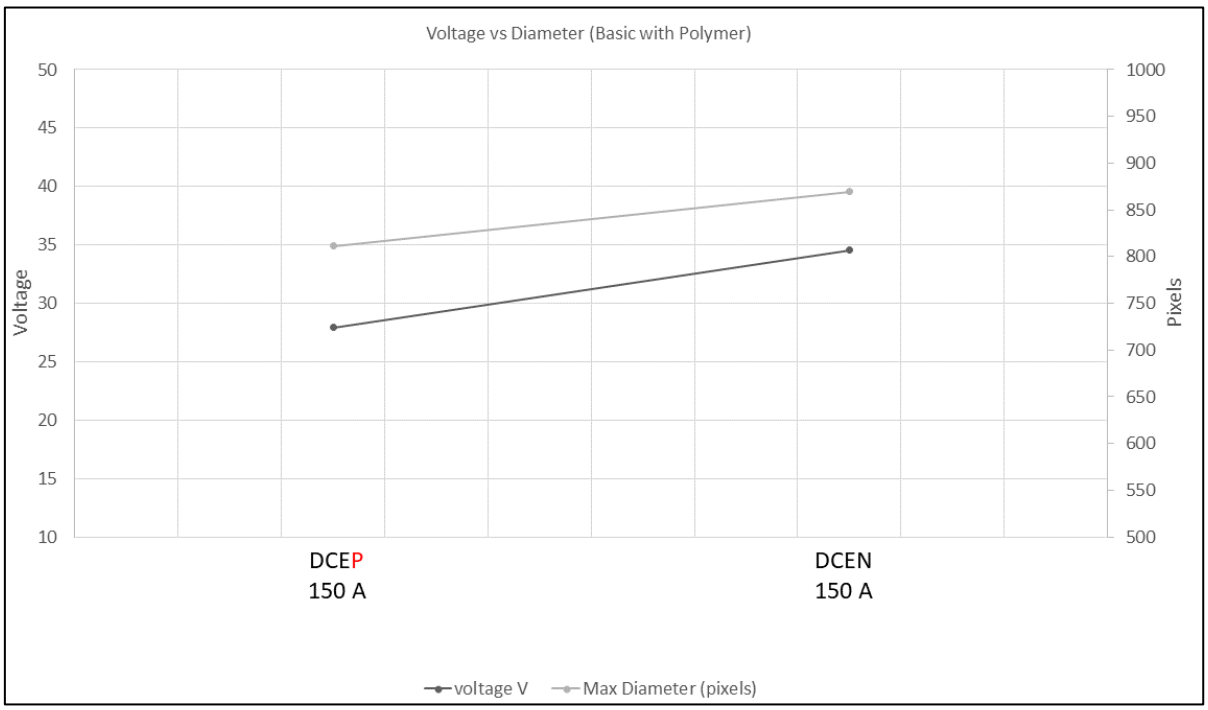

Figure A.2.2 Voltage vs Diameter.

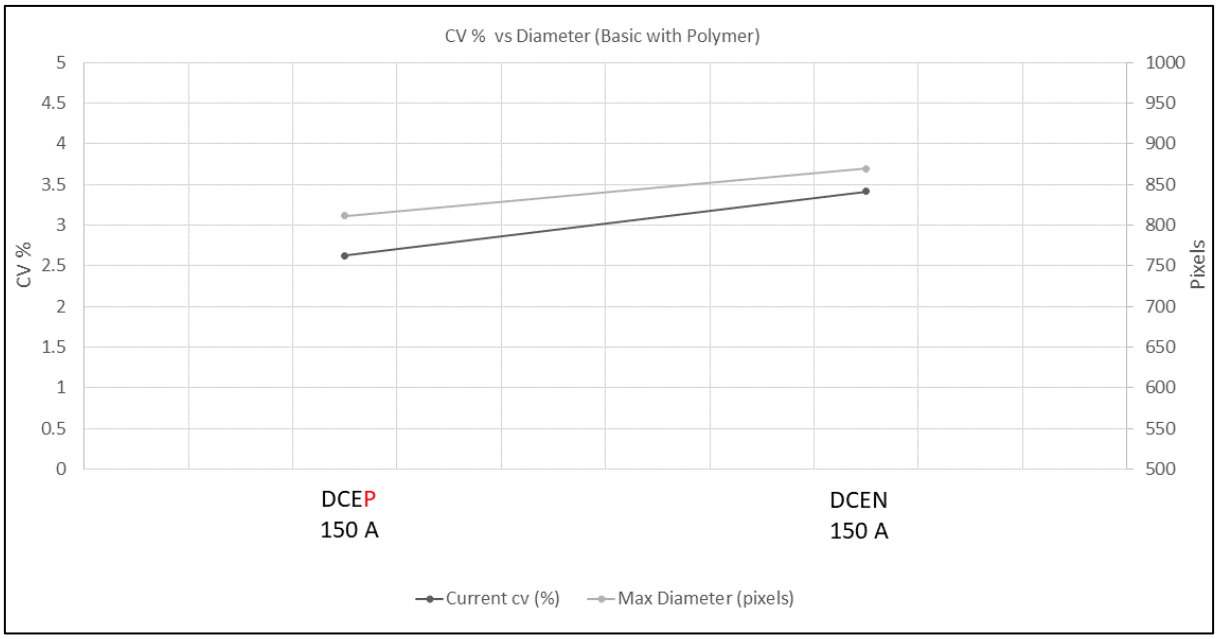

Figure A.2.3 Coefficient of variation of the current **(**CV%) vs Diameter.

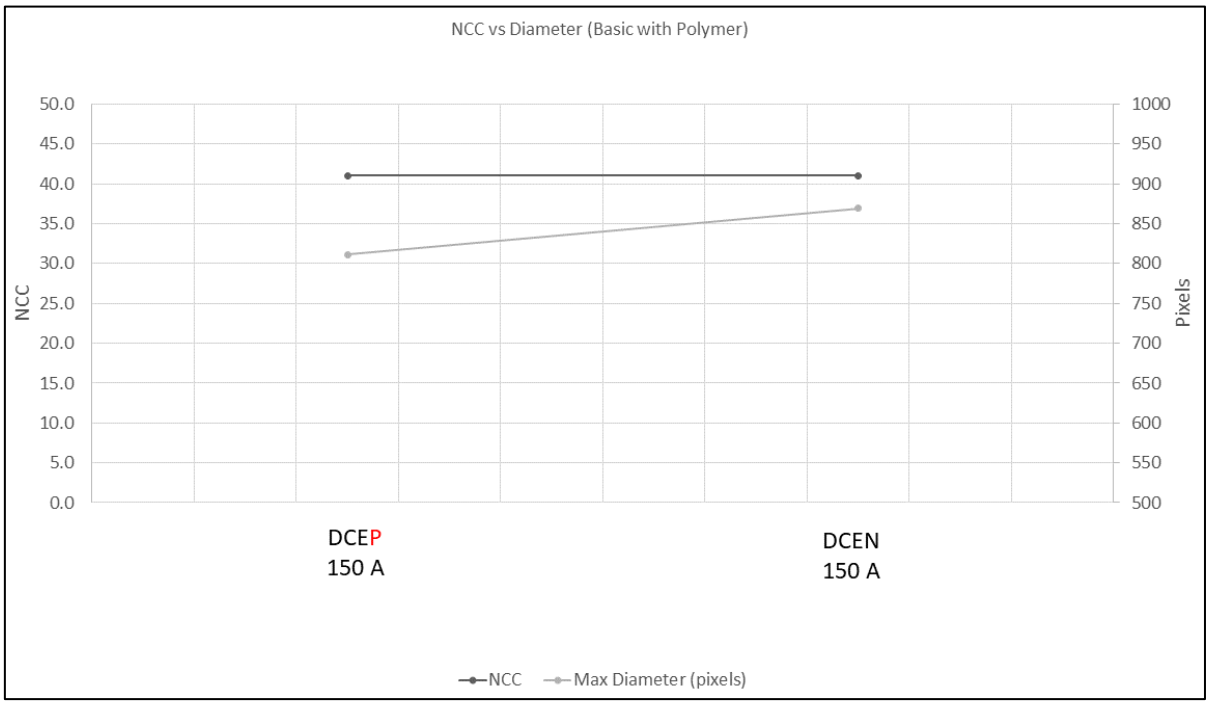

Figure A.2.4 Number of short circuits (NCC) vs Diameter.

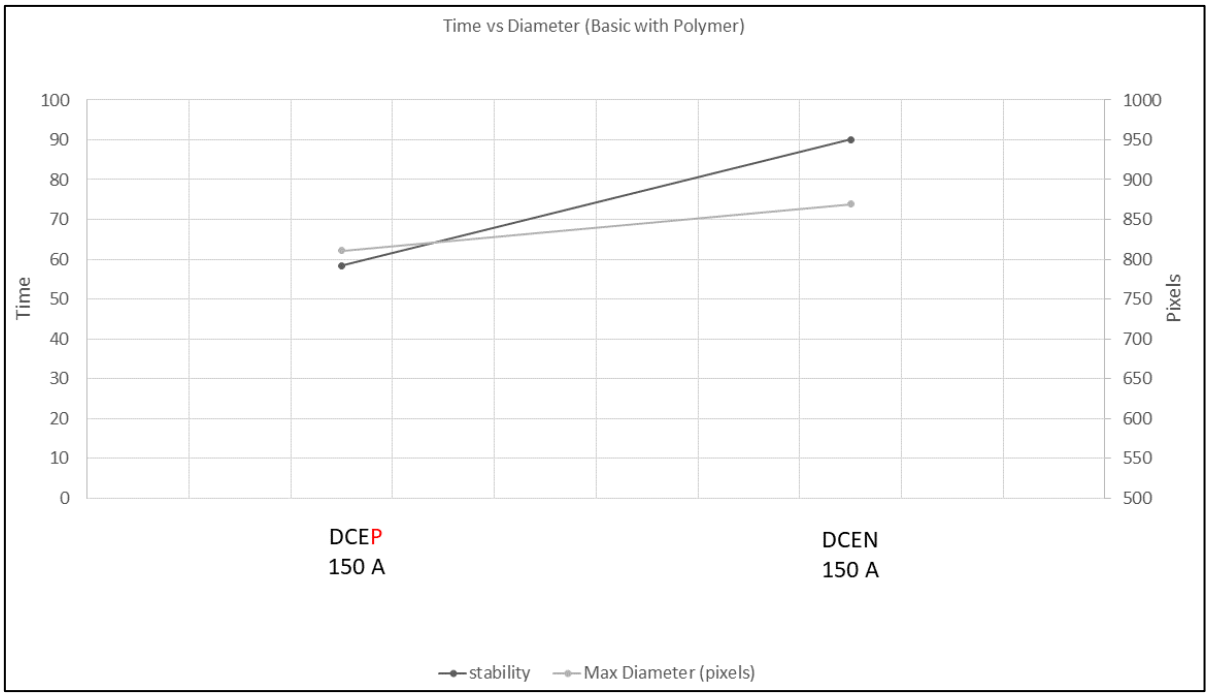

Figure A.2.5 Time remaining in the welding zone vs Diameter.

3. Rutile electrode.

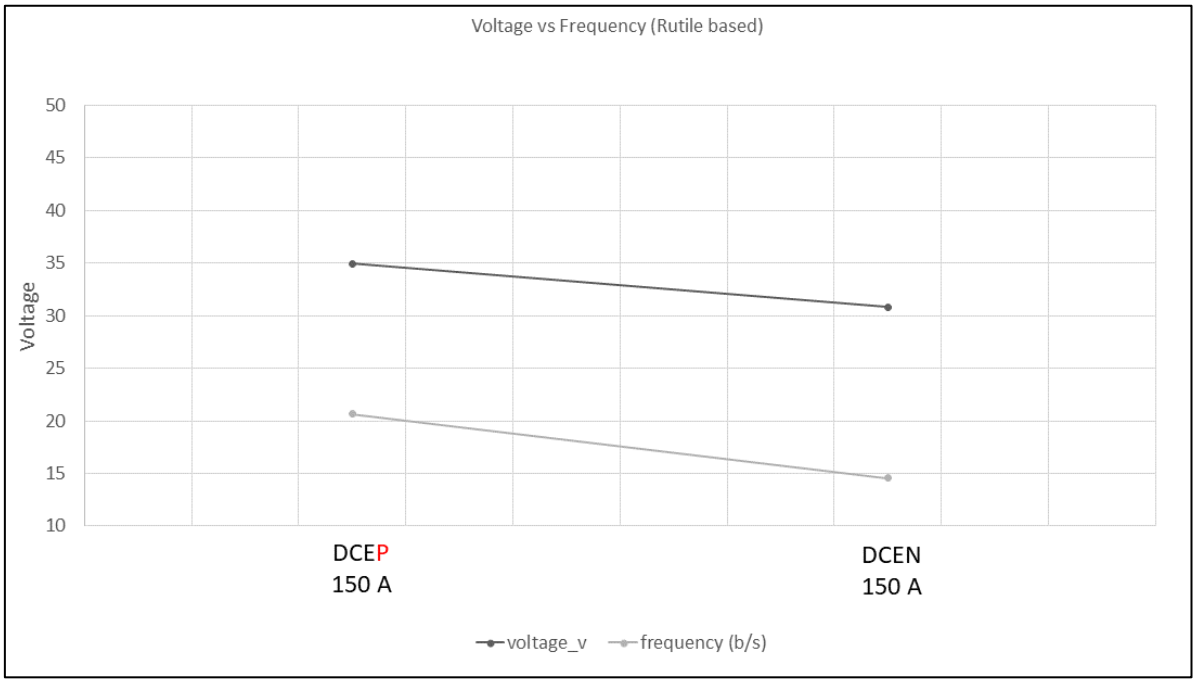

Figure A.3.1 Voltage vs Frequency.

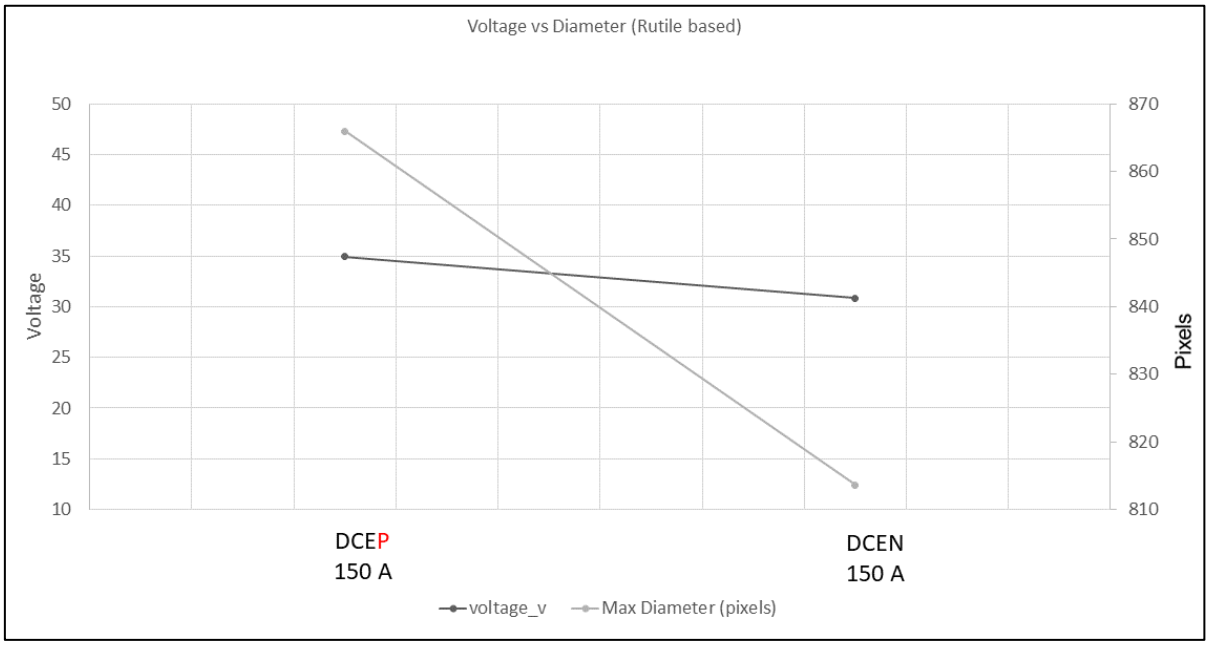

Figure A.3.2 Voltage vs Diameter.

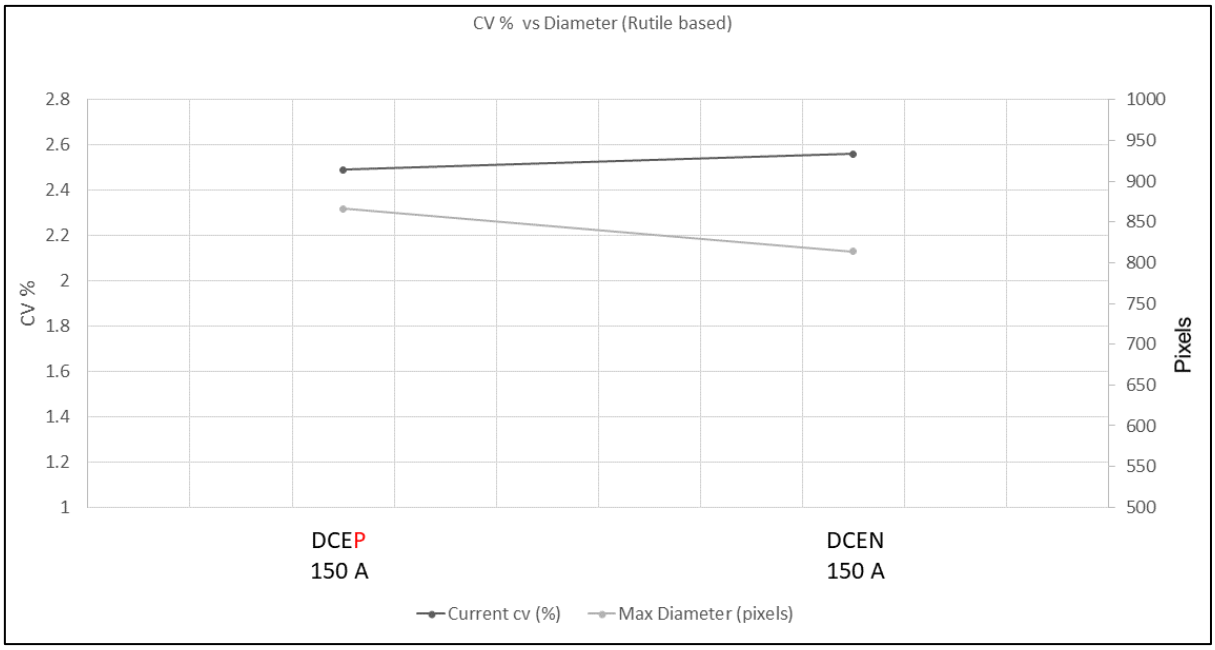

Figure A.3.3 Coefficient of variation of the current **(**CV%) vs Diameter.

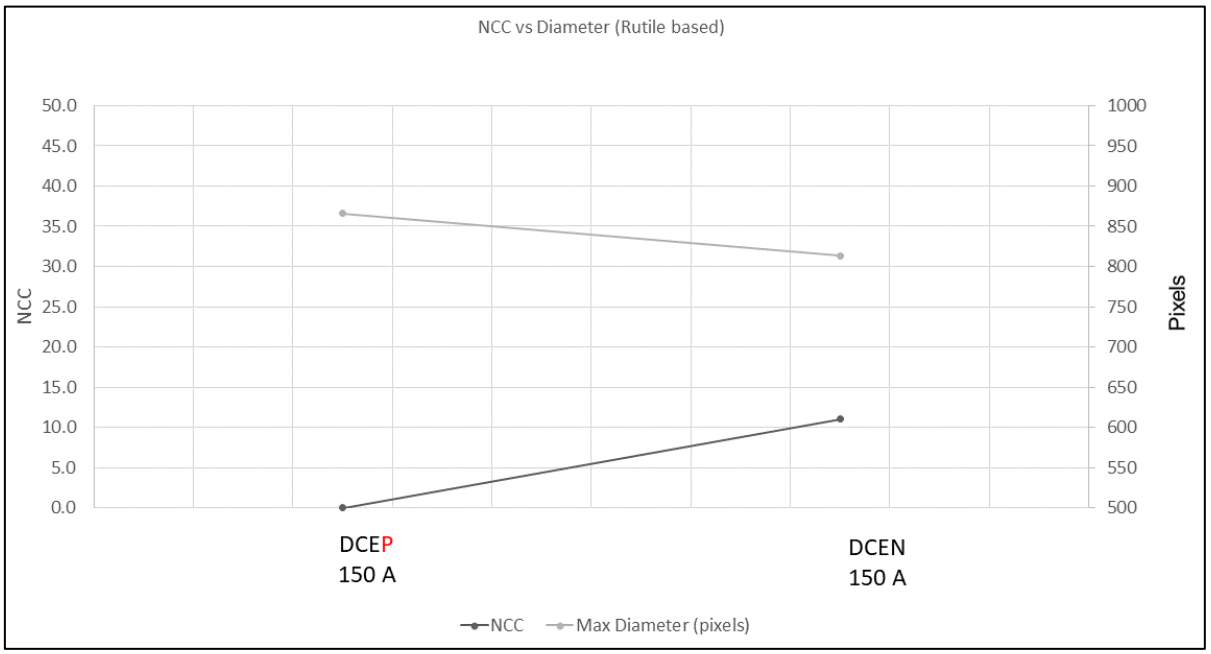

Figure A.3.4 Number of short circuits (NCC) vs Diameter.

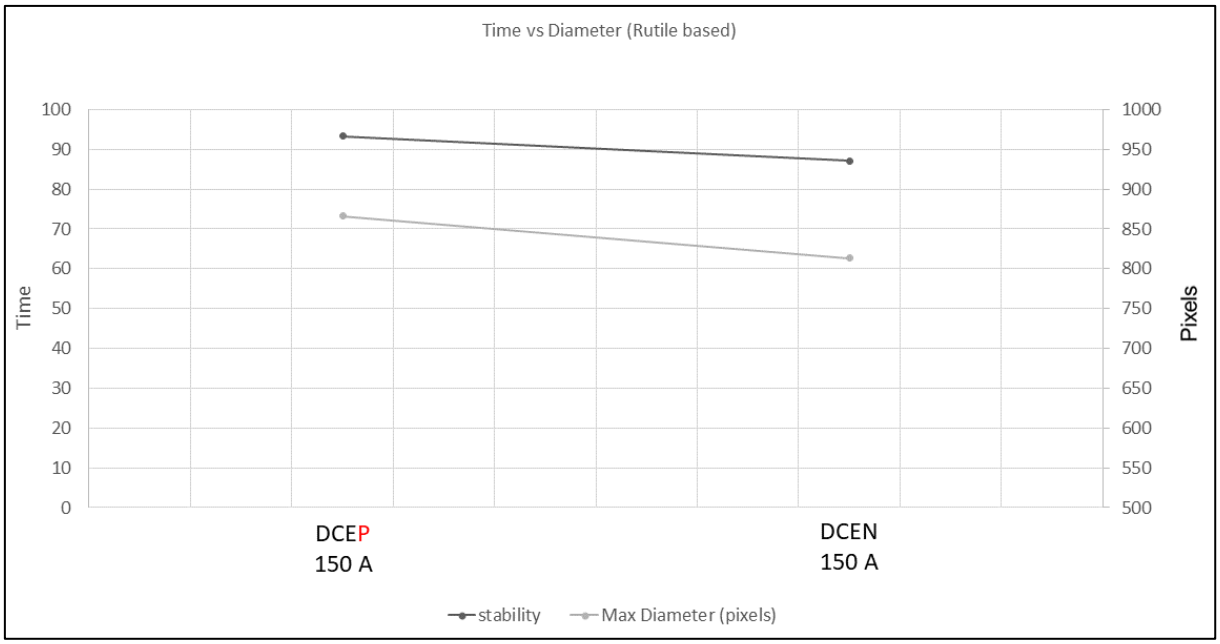

Figure A.3.5 Time remaining in the welding zone vs Diameter.

Videos Link:

https://drive.google.com/drive/folders/1hB269X71VNjwlRVvqVQlZyz6W0iV7Loh?usp=sharing